



Evolution of the Amundsen Sea Polynya, Antarctica, 2016-2021

Grant J. Macdonald, Stephen F. Ackley and Alberto M. Mestas-Nuñez

NASA Center for Advanced Measurements in Extreme Environments (CAMEE), University of Texas at San Antonio, San Antonio, TX 78249, USA

Correspondence to: Grant J. Macdonald (grant.macdonald@utsa.edu)

Abstract. Polynyas are key sites of ice production during the winter and are important sites of biological activity and carbon sequestration during the summer. The Amundsen Sea Polynya (ASP) is the fourth largest Antarctic polynya, has recorded the highest primary productivity and lies in an embayment of key oceanographic significance. However, knowledge of its dynamics, and of sub-annual variations in its area and ice production, is limited. In this study we primarily utilize Sentinel-1 SAR imagery, sea ice concentration products and climate reanalysis data, along with bathymetric data, to analyze the ASP over the period November 2016 - March 2021. Specifically, we analyze (i) qualitative changes in the ASP's characteristics and dynamics, and quantitative changes in (ii) summer polynya area, (iii) winter polynya area and ice production. From our analysis of SAR imagery we find that ice produced by the ASP becomes stuck in the vicinity of the polynya and sometimes flows back into the polynya, contributing to its closure and limiting further ice production. The polynya forms westward off a persistent chain of grounded icebergs that are located at the site of a bathymetric high. Grounded icebergs also influence the outflow of ice and facilitate the formation of a 'secondary polynya' at times. Additionally, unlike some polynyas, ice produced by the polynya flows westward after formation, along the coast and into the neighboring sea sector. During the summer and early winter, broader regional sea ice conditions can play an important role in the polynya. The polynya opens in all summers, but record-low sea ice conditions in 2016/17 cause it to become part of the open ocean. During the winter, an average of 78% of ice production occurs in April-May and September-October, but large polynya events often associated with high winds can cause ice production throughout the winter. While passive microwave data or daily sea ice concentration products remain key for analyzing variations in polynya area and ice production, we find that the ability to directly observe and qualitatively analyze the polynya at a high temporal and spatial resolution with Sentinel-1 imagery provides important insights about the behavior of the polynya that are not possible with those datasets.



1. Introduction

Coastal polynyas, or ‘latent heat polynyas’ (and henceforth referred to simply as ‘polynyas’), are sites of open water surrounded by sea ice and land, glacier ice or fast ice (Armstrong, 1972; Tamura et al., 2008; Park et al., 2018). These polynyas are distributed around the coast of Antarctica and are typically at fixed geographic locations each year. They develop because the ice that forms at these sites is regularly driven away by winds or ocean currents, creating an opening in the icepack (Bromwich and Kurtz, 1984; Bromwich et al., 1993; 1998; Morales Maqueda et al. 2004; Sansiviero et al., 2017).

Between the summer months of approximately November and March these open water sites tend to remain persistently ice-free. Among other factors, the combination of ice-free conditions, summer sunlight, and the availability of dissolved iron (e.g. Arrigo et al., 2008a; 2012; St-Laurent et al., 2017), enables large phytoplankton blooms to develop in polynyas during this summer period. These phytoplankton blooms fix carbon from dissolved carbon dioxide, some of which then sinks below the surface layer (Sweeney et al., 2003). As a result, the evolution of polynyas during the summer is considered a key factor in the primary productivity of the Southern Ocean, and consequently, also their role in the sequestration of Carbon Dioxide (the ‘biological pump’) (Arrigo et al., 2008b).

Between the winter months of approximately April and October polynyas tend to intermittently open and are smaller in area than in the summer. When a polynya does open during the winter, excess ocean heat is lost and new sea ice quickly produced. Winds (usually katabatic winds) or ocean currents then push the newly produced sea ice away and open the polynya again, producing yet more sea ice in the open area. Repeated polynya ‘events’ produce new sea ice throughout the winter period and hence polynyas have been termed ‘factories’ of sea ice production (Kimura and Wakatsuchi, 2004; Assmann et al., 2005). Overall, polynyas are estimated to contribute around 10% of all Antarctic sea ice cover (Tamura et al., 2008; Nihashi and Oshima, 2015). Regionally, polynyas can play an even larger role in production. For example, the Ross Ice Shelf polynya is estimated to produce several cubic kilometers of ice annually, and along with the McMurdo Sound Polynya, may produce 20-50% of total sea ice in the region (Drucker et al., 2011). The polynya-produced ice then forms part of the icepack, contributing to its character and potentially further thickening due to deformation. For example, ice formed by the Terra Nova Bay polynya in the Ross Sea had a mean thickness 3-4 times that of the central Ross Sea, with 80% of the study area’s ice contained in deformed ice and ridges (Rack et al., 2020). Consequently, understanding of polynya evolution through the winter is important for understanding ice production and sea ice characteristics in the Southern Ocean.

The Amundsen Sea Polynya (ASP), West Antarctica and the embayment in which it lies are of particular interest for several reasons. The polynya is situated in the embayment into which the Thwaites and Pine Island Glaciers terminate and undergo ocean-driven melting, making the oceanography of the embayment of special interest (IMBIE team, 2018; Rignot et al., 2019). The ASP is also known to be a key site of primary productivity in the summer, supporting rates of net primary production up to $2.5\text{gC m}^{-2}\text{ day}^{-1}$, the highest for any Antarctic polynya (Arrigo and Van Dijken, 2003; Arrigo et al., 2012). Additionally, the ASP has been highlighted as an important site for ice production. It has been identified as the fourth highest polynya in Antarctica in terms of area and ice production, only behind the Ross Ice Shelf, Cape Darnley, and Mertz polynyas (Tamura et al., 2008; 2016; Nihashi and Ohshima, 2015; Nihashi et al., 2017).



While there have been several recent studies of the ASP's evolution during the summer months (e.g. Arrigo et al., 2012; Stammerjohn et al., 2015; St-Laurent et al., 2019), knowledge of the ASP and its role in ice production during the winter is limited. Additionally, few studies during the summer have analyzed changes at the sub-monthly scale, and none have observed the polynya directly during cloudy conditions. Aside from one study that analyzed the ASP at the mean monthly scale (Tamura et al., 2016), studies that analyze ice production in the ASP during the winter have been limited to estimates of total annual ice production and mean annual area as part of broader-scale circum-Antarctic studies (Tamura et al., 2008; Nihashi and Ohshima, 2015; Nihashi et al., 2017). Other studies of the ASP during the winter have focused on other aspects of the polynya, such as iron and carbon fluxes (St-Laurent et al., 2019). There are a lack of studies of the polynya that characterize changes in the polynya's evolution and area through individual seasons. This is partly due to the difficulty of analyzing polynyas in detail during the polar night. However, the launch of the Sentinel-1 constellation of Synthetic Aperture Radar (SAR) - in full operation by May 2016 - enables us to directly observe the polynya during the polar night at a high spatial resolution. Additionally, during the summer light, SAR allows us to make observations regardless of cloud cover.

The overall goal of the work presented here is to improve knowledge of the behavior and evolution of the ASP, and thus to aid understanding of recent complex and poorly understood trends in Southern Ocean sea ice conditions. This in turn, will aid predictions of future changes in Southern Ocean sea condition due to climate change, with important consequences for a range of processes, such as Antarctic bottom water formation and global thermohaline circulation (Orsi et al., 1999; Krumpen et al., 2011; Tamura et al., 2012; Ohshima et al., 2013; Kitade et al., 2014; Marzocchi and Jansen, 2019), Antarctic Ice Sheet stability (Banwell et al., 2017; Webber et al., 2017; Greene et al., 2018; Massom et al., 2018; Arthur et al., 2021) and ecosystem productivity (Grossman and Dieckmann, 1994; Ito et al., 2017). The three specific objectives of this paper are to, over the period November 2016 - March 2021, analyze seasonal and inter-annual (i) qualitative changes in the ASP's characteristics and dynamics, and quantitative changes in (ii) summer polynya area and (iii) winter polynya area and ice production. The main datasets used are Sentinel-1 SAR images, sea ice concentration products, and climate reanalysis data in the region of the ASP. Additionally, we analyze bathymetric data, and changes in the broader regional sea ice.

2. Study Site

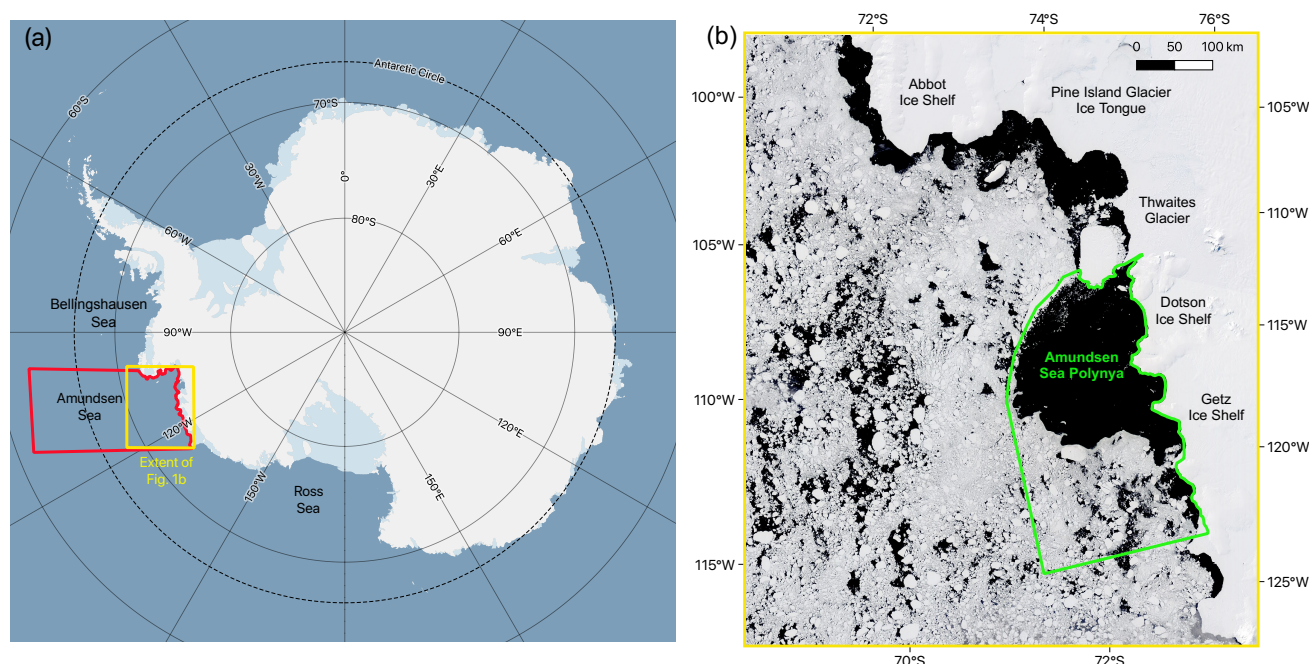
The ASP is located at around $\sim 72\text{--}73^\circ\text{S}$ and $110\text{--}120^\circ\text{W}$ in the Amundsen Sea embayment of the Southern Ocean in West Antarctica (Fig. 1). It is situated in a sector that exhibited an anomalous 40-year decreasing trend in sea ice extent until a 2007 minimum, since which there has been an increasing trend (Parkinson, 2019). To the east, the polynya is bound by the Thwaites Iceberg Tongue and a chain of icebergs. To the south, when at its maximum extent, the polynya abuts the Dotson Ice Shelf and part of the Getz Ice Shelf. Immediately east of the eastern boundary of the polynya is an area of ocean that is adjacent to Thwaites Glacier and Pine Island Glacier. The neighboring 'Pine Island Polynya' forms along the coastal stretch around this area and to the north. Westward coastal currents prevail in the area (St-Laurent et al., 2019), that, along with easterly winds, carry icebergs (Koo et al., in review) and sea ice into the adjacent sector or the Amundsen Sea and eventually to the Ross Sea (Assmann et al., 2005).



110 The ASP opened every summer during the period 1979-2014 studied by Stammerjohn et al. (2015) and re-
111 tained some open polynya area through the winter period. Arrigo et al. (2012) found no significant secular trend in
112 mean summer open water area between 1997 and 2010, but Stammerjohn et al. (2015) did find the ASP's area in
113 December-February to increase overall over the period 1979-2014. They also noted that the site of the polynya
114 opening shifted to its current typical site adjacent to the Thwaites Glacier Tongue in 1993, having previously been
115 further to the west.

116 Synoptic-scale winds have been found to primarily determine the ASP's area and the timing of opening and
117 closure. Over the period 1997-2010, ASP area was greatest in the summers of 2002-03 and 2009-10, the years with
118 the largest monthly anomalies in easterly and southerly surface winds in the region, and smallest in 2003-04 when
119 there were anomalously high northerly and westerly winds (Arrigo et al., 2012). Polynya opening in November was
120 associated with prevailing easterly or southeasterly winds, while closure in March was associated with persistent
121 southeasterly winds at a time when winds promote ice growth in open areas. The polynya was also found to open 16
122 ± 7 days earlier at the end of the period 1979/80-2013/14 than the beginning (Stammerjohn et al., 2015).

123 During the winter, the polynya's area was estimated to have a daily mean of $7700 \pm 3600 \text{ km}^2$ for the pe-
124 riod March-October, 2003-11, as estimated from Advanced Microwave Scanning Radiometer for EOS (AMSR-E)
125 data (Nihashi and Ohshima, 2015). Annual ice production has been estimated as $92 \pm 16 \text{ km}^3$ for the period 1992-
126 2001 (Tamura et al., 2008) and $123 \pm 24 \text{ km}^3$ for the period 1992-2013 (Tamura et al., 2016) using Special Sensor
127 Microwave/Imager (SSM/I) data. Nihashi et al., 2017 estimated annual ice production as $90 \pm 13 \text{ km}^3$ (AMSR-E
128 data) for the period 2003-10, and $90 \pm 17 \text{ km}^3$ (AMSR2) for the period 2013-15.



129



Fig. 1. (a) The location of the Amundsen Sea and our study sites within the context of Antarctica and the Southern Ocean. The background image is from Quantarctica (Matsuoka et al., 2021); (b) The location of the ASP within the Amundsen Sea embayment. The green boundary indicates the area defined as the ‘ASP study area’ for the purpose of calculating winter polynya area and ice production. The background image is a true-color MODIS image from 12 December 2020.

3. Data & Methods

3.1 Qualitative analysis of the ASP’s evolution

In order to qualitatively characterize the seasonal and interannual evolution of the ASP we use Sentinel-1 SAR imagery. Sentinel-1 is a constellation of two satellites, A and B, that were launched by the European Space Agency (ESA) in 2014 and 2016, respectively. The satellite collects radar backscatter imagery in the C-band which allows observations of sea ice and the ocean during cloudy conditions and the polar night.

For our analysis we processed all Sentinel-1 extra-wide swath (EW) mode, Ground Range Detected (GRD) images over the study site and its surroundings (Fig. 1b) for the period November 2016 to March 2021. This period was chosen because it includes all the complete summer (November–March) and winter (April–October) periods during which both satellites A and B of the Sentinel-1 SAR constellation have been active. The EW mode was primarily designed for sea ice and polar zones and collects images over a wider area than other modes. EW images are available in 20m x 40m spatial resolution and all images were resampled to 40 m grid spacing. Of four available band combinations (VV, HH, VV+VH, and HH+HV), we use the HH band because most of the images contain this band. Using these images, we created a time-lapse animation using Google Earth Engine. This time-lapse included at least partial coverage of the study area for 56 days in 2016, 359 days in 2017, 341 days in 2018, 317 days in 2019, 329 days in 2020 and 85 days in 2021. In order to analyze particular images in detail, the images were also downloaded from the Alaska Satellite Facility (asf.alaska.edu) and processed in ESA’s ‘SNAP’ toolbox. SNAP was used to crop the images, apply radiometric correction, speckle filtering and ellipsoid correction and convert the images to decibel values. The images were then loaded into QGIS (QGIS.org, 2021) for analysis.

Qualitative analysis was carried out by visually analyzing the time-lapse videos and images of interest, noting changes in the state of the polynya and ice in the region. Visual analysis is possible because of the distinct backscatter signals and texture of open water and different types of sea ice. Typically, open ocean water has a low backscatter and appears dark, while thicker, older icepack has a relatively high backscatter and appears bright and more granular (we refer to all ice not produced by the ASP as ‘icepack’) (Fig. 2a–b). Recently-formed polynya-produced ice has an intermediate backscatter (Fig. 2a). Frazil ice, that may form when a polynya opens up and the open ocean begins to freeze, forms in distinct bands of varying brightness (Fig. 2c–d).

Given the role grounded icebergs play in bounding the ASP, we also downloaded the ‘BedMachine Antarctica V2’ sea floor topography dataset for our study area to examine alongside our qualitative analysis. This dataset was downloaded from the NSIDC (<https://nsidc.org/data/nsidc-0756>) and has a grid spacing of 500 x 500 m (Morlighem et al., 2020).

We also use our analysis of the imagery to assess the approximate day of summer polynya ‘opening’ and ‘closing’. We deem the polynya to be open for the summer when the open polynya area is primarily free of active ice production, and the day of summer closing to be when the whole open polynya is subject to ice production.



169

170 3.2 Daily polynya area

171 In order to analyze seasonal and interannual changes in polynya area in summer and winter, daily sea ice
 172 concentration (SIC) for the study region was downloaded from the University of Bremen's sea ice data center
 173 (seaice.uni-bremen.de). The data was separated into five summer periods from November to March (2016/17,
 174 2017/18, 2018/19, 2019/20 2020/21) and four winter periods from April to October (2017, 2018, 2019, 2020). This
 175 time period was focused on because it coincides with the period for which there is Sentinel-1 A and B data. We
 176 begin our winter period in April rather than March because analysis of the Sentinel-1 imagery suggests ice produc-
 177 tion is not active across the open polynya at the beginning of March. The sea ice concentration product was pro-
 178 cessed by the University of Bremen using the ARTIST Sea Ice (ASIC) algorithm (Spreen et al, 2008) applied to
 179 AMSR-2 data. AMSR-2 was launched onboard the Japan Aerospace Exploration Agency's (JAXA) Global Change
 180 Observation Mission - Water (GCOM-W) satellite in July 2012.

181 We used version 5.4 of the Antarctic-wide, daily sea ice concentration product with no land mask, pro-
 182 cessed to 3.125 km grid spacing. This is of a higher-resolution than data previously used to analyze polynya area in
 183 the region. For example, Arrigo et al., (2012) used SSM/I data with 6.25 km grid spacing for their study of summer
 184 polynya area. Nihashi et al. (2017) used AMSR-E data with 6.25 km grid spacing for their estimates of ice produc-
 185 tion. Tamura et al. (2008; 2016) also used SSM/I data, with 12.5 km grid spacing, for estimates of ice production.
 186 Stammerjohn et al. (2015) used Bootstrap SIC data with 25 km grid spacing for their analysis of summer polynya
 187 area. However, with our higher-resolution data (3.125 km) there remain limitations in using data with such a scale to
 188 measure something that can vary on a meterscale. It has been estimated that the ice concentration error in our
 189 AMSR-2 dataset is 25% at 0% SIC, decreasing to <10% error for SIC over 65% and 5.7% error at 100% SIC
 190 (Spreen et al., 2008). Data was available for all days in our study period apart from one day in 2019 (1 September).

191 After each day's data was downloaded as a geotiff, it was cropped to the 70 660 km² ASP study area de-
 192 fined in Fig. 1b using a shapefile drawn in QGIS with a Sentinel-1 image as reference. Polynya area was then calcu-
 193 lated by defining any pixel in the study area with a SIC < 70% as being part of the open polynya. The 70% threshold
 194 has been commonly used in other studies of polynyas (e.g. Parmiggiani, 2006; Morelli & Parmiggiani, 2013;
 195 Preußner et al., 2015). A limitation is that smaller areas of open water that are represented in a pixel dominated by
 196 ice-covered area (i.e. > 70%) will not be included in our polynya area value, while ice-covered areas in pixels with
 197 SIC < 70% will be included. However, based on visual comparison with coincident Sentinel-1 imagery, we found
 198 70% to be an appropriate threshold for accurately estimating open polynya area.

199 While Sentinel-1 imagery has been used to obtain polynya area during the polar night at a higher spatial
 200 resolution (40m, Dai et al., 2020), the Bremen SIC product has three key advantages over using Sentinel-1 SAR im-
 201 agery. First, the SIC product is available daily, in contrast to Sentinel-1 which has many, and sometimes prolonged
 202 data gaps over the primary area of interest, particularly during June/July. Given that polynya area can change sub-
 203 stantially on a daily or hourly timescale, regular gaps of successive days significantly limits the ability to quantita-
 204 tively characterize variations throughout the year. Second, several Sentinel-1 images are required to capture the
 205 whole ASP study area on a particular day, meaning that even on many days where there are images that are useful



for qualitative analysis, the whole polynya cannot be measured. For example, in 2020 there is full coverage for only 22 days with none between 26 April and 12 August. Third, even if sufficient images were available, current methods for calculating polynya area in Sentinel-1 imagery (e.g. Dai et al., 2020) requires manual delimitation which is labor intensive and would be highly time consuming to do for multiple years at a daily temporal resolution.

3.3 Daily winter ice production

In order to calculate daily ice production in the ASP during the winter periods we applied a heat flux and ice production model following Cheng et al. (2017). As input we used climate re-analysis data from the European Centre for Medium-Range Weather Forecasts Reanalysis v5 (ERA5) model and the same sea ice concentration data from the University of Bremen described in section 3.2.

Hourly ERA5 data, with a spatial resolution of 31 km, was downloaded from Copernicus (cds.climate.copernicus.eu; Herbach et al., 2018) for the following meteorological variables: air temperature at a height of 2 m, wind speed at a height of 10 m, surface air pressure, dewpoint temperature at a height of 2 m, downward solar radiation and downward thermal radiation. Air temperature, wind speed, surface air pressure and dewpoint temperature were then processed to daily mean values, while solar and thermal radiation were processed to daily cumulative values. These calculations were done for the same ASP study site as for polynya area (Fig. 1b).

3.3.1 Heat Flux Calculation

Following Cheng et al. (2017) the daily net heat flux, Q (in Wm^{-2}), of a pixel was estimated by:

$$Q = (1 - \alpha)S_i + L_i - L_o + F_s + F_e \quad (1)$$

where S_i (in Wm^{-2}) is the cumulative downward solar radiation; L_i (in Wm^{-2}) is the cumulative downward thermal radiation; L_o (in Wm^{-2}) is the upward thermal radiation; F_s (in Wm^{-2}) and F_e (in Wm^{-2}) are the sensible heat flux and latent heat flux, respectively; and α is the albedo of open water. α was taken to be 0.06 following Cheng et al. (2017; 2019), S_i and L_i were taken from the processed daily ERA5 values and L_o , F_s and F_e were calculated as described below.

The upward thermal radiation was calculated by the Stefan-Boltzmann law:

$$L_o = \varepsilon \sigma T_0^4 \quad (2)$$

where ε is the longwave emissivity of open water (0.99), and σ is the Stefan-Boltzmann constant ($5.67 \times 10^{-8} \text{ W}^{-2}\text{K}^{-4}$). T_0 (in K), the freezing point of seawater, was assumed to be the temperature of the water surface (T_s , in K), which was calculated following Motoi et al. (1987) and Cheng et al. (2017; 2019) as:

$$T_0 = T_s = 273.15 - 0.0137 - 0.05199s_w - 0.00007225s_w \quad (3)$$



where sw (in ‰) is the salinity of sea water. The salinity of the Amundsen Sea was estimated as 34‰ based on Bett et al. (2020).

The sensible heat flux, (F_s), and latent heat flux, (F_e) was calculated by:

$$F_s = \rho_a c_p C_s U (T_a - T_0) \quad (4)$$

and

$$F_e = 0.622 \rho_a L_v C_e U (r e_a - e_s) / P_0 \quad (5)$$

where ρ_a is the density of air at standard atmospheric pressure and 0°C, taken as, $1.3 \text{ kg} \cdot \text{m}^{-3}$, c_p is the specific heat of air at constant pressure, taken as $1004 \text{ J kg}^{-1} \text{ K}^{-1}$, U (in ms^{-1}) is the wind speed at 10 m, taken from the processed ERA5 data and T_a (in K) is the air temperature at 2 m, taken from the processed ERA5 data. C_s and C_e are bulk transfer coefficients for sensible heat and latent heat, respectively and both taken as 0.00144. P_0 (in pa) is the surface air pressure and taken from the processed ERA5 data. L_v (in J kg^{-1}) is the latent heat of water vaporization, r is the relative humidity. e_a (in pa) is the saturation water vapor pressure at the air temperature, $r e_a$ is the actual water vapor pressure of the air and e_s (in pa) is the saturated water vapor pressure at the surface temperature and are all calculated below:

$$L_v = [2.501 - 0.00237(T_s - 273.15)] \times 10^6 \quad (6),$$

$$e_s = 6.11.21 \times 10^{9.8094(T_s - 273.15)/(T_s + 0.71)} \quad (7),$$

and

$$r e_a = 611.21 \times 10^{9.8094(T_d - 273.15)/(T_d + 0.71)} \quad (8)$$

where T_d is the dewpoint temperature taken from the processed ERA5 data.

3.3.2 Ice production calculation

The calculated daily heat flux was then cropped, re-aligned, resampled to a 3.125 km^2 grid and reprojected to Antarctic Polar Stereographic using GDAL and QGIS to match the corresponding sea ice concentration data. Next, where SIC was < 0.7 (i.e. pixels considered as part of open polynya) daily ice production volume, V , was estimated in km^3 following Cheng et al. (2017) by the following equation (9). Although ice production will also take place in areas where there is ice cover, here we are only concerned with ice production taking place in the open polynya.



$$V = 3.125^2(1-SIC)Q/\rho L_f \quad (9)$$

where, as above, SIC is sea ice concentration (as a fraction) and Q is daily net heat flux in W m^{-2} , ρ is sea ice density and taken as 920 kg m^{-3} and L_f is the latent heat of sea ice fusion in J kg^{-1} . L_f is calculated following Moham-
 med and Nirmal (2015) and Cheng et al. (2017) by:

$$L_f = 333400 - 2113(T_0 - 273.15) - 114s_i + 18040s_i/(T_0 - 273.15) + 3.35s_i(T_0 - 273.15) - 3.76(T_0 - 273.15)^2 \quad (10)$$

where s_i is the salinity of sea ice, taken as 6‰ following Cheng et al. (2017).

Caution should be used when interpreting the absolute numbers produced by the ice production model, particularly because the input data is modeled climate data not necessarily always representative of reality, and the model itself is a simulation sensitive to uncertain parameter settings (Cheng et al., 2017; 2019). Nevertheless, we opted for this method due to the difficulty of directly measuring and tracking thin ice thickness in the polynya (e.g. Tian et al., 2020) to estimate ice production, and the potential to compare our daily ice production results to results obtained by the same model for the Ross Ice Shelf Polynya (Cheng et al., 2017; 2019).

3.4 Broader spatial changes in SIC

In order to assess changes in the ASP in the context of changes in SIC at a broader spatial scale, SIC was analyzed for the larger area defined in Fig. 1a. The same SIC dataset described in section 2.2 to obtain polynya area was cropped to the broader region. The daily data was plotted spatially for all available days 1 November 2016 - 31 March 2021, as shown in Video S2. Monthly mean SIC was also calculated for the whole period and plotted spatially. Additionally, the total SIC for each day was calculated by calculating the sum of all percentage SIC values in the study region. These total SIC values should only be considered useful for analyzing relative changes in SIC in our study period.

3.5 Wind speed and direction

In order to analyze how polynya behavior relates to changes in wind conditions, mean wind speed and direction, and daily wind speed was calculated from ERA5 wind data. To obtain mean wind speed and direction, ERA5's monthly wind speed and direction product was downloaded and cropped to the ASP study area (Fig. 1b) for the period 1 November 2016 to 31 December 2020 and the mean calculated for the whole period, and plotted spatially.

Daily wind speed and direction at the site of the polynya, ERA5's hourly 'u' and 'v' wind products were processed for a region adjacent to the Dotson Ice Shelf and iceberg chain where the polynya typically forms, identified in Fig. S1. Hourly wind speed in ms^{-1} , V , was calculated as

$$V = (u^2 + v^2)^{1/2} \quad (11)$$



where u and v are ERA5's u and v 10 m wind products, respectively. Daily wind speed and direction was also plotted spatially for the study area, included as supplementary video Video S3. For this, wind direction was plotted using the 'matplotlib' function 'quiver'.

Unfortunately there is a lack of local observations of wind data, and the closest station in the United States Antarctic Program's database, on Bear Peninsula, lacks wind data for most of our study period. As a result, some caution should be employed when considering these results. However, Bracegirdle (2013) and Stammerjohn et al. (2015) note that data from ERA5's predecessor ERA-I in the neighboring Bellingshausen Sea performed better than other reanalysis products.

4. Results

In this section, we first describe our qualitative analysis of the Sentinel-1 SAR imagery of the ASP between November 2016 and March 2021 (Section 4.1). Second, we analyze quantitative changes in summer (November - March) polynya area for the summers of 2016/17 to 2020/21 (Section 4.2). Third, we analyze quantitative changes in winter (April - October) polynya area and winter ice production for the winters of 2017 to 2020 (Section 4.3). Fourth, we analyze spatial and temporal variations in wind speed and how they relate to polynya area (Section 4.4), and finally, we analyze broader regional patterns in sea ice concentration for the period November 2016 - March 2021 (Section 4.5).

4.1 Qualitative analysis of ASP using Sentinel-1 SAR imagery

4.1.1 November 2016 - December 2017

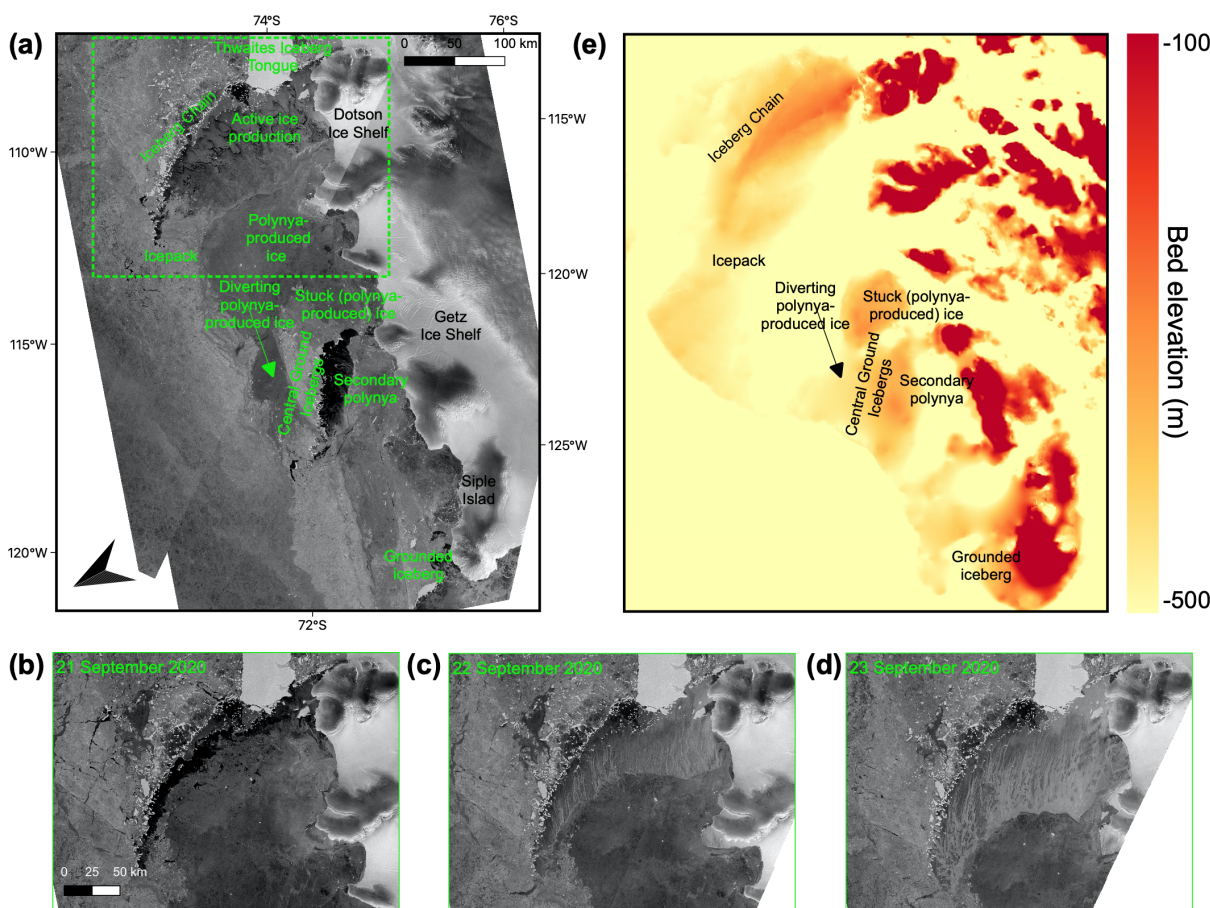
By the time of the first clear image of the ASP on 14 November 2016 the polynya is already open for the summer, adjacent to the Iceberg Chain and the Dotson Ice Shelf, as well as part of the Getz Ice Shelf (Video S1). Through November and December, the polynya continues to extend westward. It also extends northward in the area west of the Iceberg Chain. In late December and early January the Pine Island Polynya to the east has also extended westward. Loss of most of the fast ice and icepack around the Iceberg Chain through the remainder of the summer means that only the presence of the Iceberg Chain delineates the boundary between the two polynyas for part of the summer. Additionally, by early January the icepack that typically bounds the polynya to the north is no longer present, so the western area of the polynya has no northern limit and is congruent with the open ocean.

From around 13 February 2017 a narrow band of icepack from the north-west begins to drift around the Iceberg Chain into the polynya, until by 3 March the polynya is once again isolated and bound to the west by the narrow band of icepack. By late March new ice is forming in the polynya, until by approximately 4 April 2017 any open polynya area appears to be the site of ice production, and we consider the summer phase of the polynya to be 'closed' (Table 1). To the east and north-east ice production is also taking place in the Pine Island Polynya, and icepack that has drifted from the Bellingshausen Sea fills the western side of the Pine Island Polynya, adjacent to the Abbott Ice Shelf.

From April 2017 onwards, numerous polynya events take place. During these events ice in the polynya typically blows to the west, creating an opening in the polynya adjacent to all or part of the Iceberg Chain. New ice can



354 be seen forming in this opening, typically as frazil bands, which sometimes form in approximately parallel bands
355 (e.g. Fig. 2c-d). Otherwise, ice production sometimes forms a ‘swirl’ of thin ice. Alternatively, at times ice drifts
356 northward from the Dotson Ice Shelf or Bear Peninsula and new ice forms adjacent to those sections while parts ad-
357 jacent to the Iceberg Chain remain closed. From April through August the polynya never extends further west than
358 the western margin of the Dotson Ice Shelf. However, separate ‘mini polynyas’ within our ASP study area can be
359 seen forming along the coast, particularly to the west, and sometimes north, from the rock outcrops between outlets
360 of the Getz Ice Shelf.



361 **Fig. 2.** (a) An example image of the ASP during the winter in a Sentinel-1 SAR image from 5 September 2019. (b-
362 d) An example of a polynya event taking place 21-23 September 2020 in Sentinel-1 SAR imagery. The area corre-
363 sponds to the dashed-green box in (a). (e) The elevation of the bed referenced to mean sea level for the same area as
364 (a). The bathymetry data is from the MEaSUREs BedMachine version 2 dataset (Morlighem et al., 2019).
365



From April through August 2017, new ice formed by the polynya extends and drifts westward overall, eventually rounding the corner of Siple Island. However, the ice does not consistently flow westward from the polynya. The ice often ‘heaves’ from the polynya, traveling westward overall but often reversing direction and temporarily drifting back towards the polynya. When the polynya opens, it may then close due to new ice formation or because polynya-produced ice drifts back into the open area.

The flow of ice out of the study area is also disrupted by areas of ice that get stuck and prevent new ice from drifting westward along the coast. Between April and August an area of ice becomes stuck as it becomes fast to the east of some grounded icebergs off the Siple Island coast. This forces ice to divert around as it rounds the corner of Siple Island. Ice also intermittently gets stuck/fast in a region around the center of the ASP study area we call the ‘Central Grounded Icebergs’ (Fig 2a), which corresponds to a topographic high in the sea floor (Fig. 2e). The obstruction caused by this section of ice causes the polynya-produced ice to flow north around the Central Grounded Icebergs, leading to a substantial northward extension of polynya-produced ice, particularly in September-October.

From October larger polynya events begin to take place. For example, on 5 October and 25 October areas of open water occupied by newly-forming ice extend from the Iceberg Chain at least as far west as the eastern outlet of Getz Ice Shelf. In the latter part of November, the polynya opens and remains open, although ice production visibly takes place in some of the open area. By early December there is little evidence of ice production (Table 1) and through December the western boundary of the polynya progressively drifts to the west and north-west, extending the polynya.

4.1.2 January - December 2018

Through the summer of 2017/18 (Video S1) the ocean to the north is occupied by more icepack than in 2016/17 and therefore the polynya always has a northern boundary. However, through January the western boundary migrates westward so that by early February it is outside our study area, if it remains at all. A gap in the icepack also connects the polynya to the open ocean in the north-west of our study area. Compared to the previous year, a more substantial section of icepack and fast ice separates the ASP from the Pine Island Polynya throughout the whole summer.

By late February the polynya is contained within the ASP study area, extending along the entire coast of this area. There is also evidence of ice production in parts of the polynya around this time. By around 9 March 2018 ice production is taking place across the polynya area (Table 1) and the open area gets progressively smaller through March and April, apart from during some polynya events. For example, a large event around 14 April takes place that extends from the eastern boundary to the second-most eastern outlet of the Getz Ice Shelf.

The polynya then behaves in a similar way to the previous year, with polynya events occurring throughout the winter, and blockages of ice by the two grounded iceberg regions (next to Siple Island and the Central Grounded Icebergs) influencing the evacuation of new polynya-produced ice from the area. The ice that gets stuck in these areas is sometimes new polynya-produced ice and sometimes icepack that drifts in from the north-east. Some of this ice appears to be formed in the Pine Island Polynya and some drifts in from the Bellingshausen Sea sector. When this icepack comes into the polynya region, it appears to sometimes play a role in pushing newly formed ice back



into the open polynya when it ‘heaves’ and closes. By mid-November ice production appears to mostly cease and the polynya opens up further through November and December (Table 1).

4.1.3 January - December 2019

As in the previous year, a more substantial icepack than in 2016/17 exists to the north of the ASP through the summer of 2018/19. However, in the summer of 2018/19 this icepack connects with the coast, giving the ASP a western limit and keeping the ASP isolated from the open ocean throughout the summer. Compared to the previous year, the neighboring Pine Island Polynya extends closer to the ASP but a section of ice fast along the eastern side of the Iceberg Chain maintains a clear boundary between the two polynyas. Through February the icepack flows around the Iceberg Chain and in from the north, reducing the polynya’s area. By 14 March 2019 new ice or forming ice is visible across the whole polynya (Table 1). From then the polynya behaves in a similar manner to the previous two years.

Year	Polynya opens	Polynya closes
2016/17	8 November 2016*	4 April 2017
2017/18	3 December 2017	9 March 2018
2018/19	13 November 2018	14 March 2019
2019/20	20 November 2019	21 March 2020
2020/21	16 November 2020	8 March 2021

Table 1. Summer polynya opening and closing dates for each summer 2016/17-2020/21 as determined by visual analysis of Sentinel-1 SAR imagery. We determine the polynya to be open for summer when the majority of the open polynya is not exhibiting ice production and closed when the majority of the polynya is exhibiting ice production. * in 2016/17 a lack of imagery in early November means it is difficult to determine when the polynya opened, but it is open by 8 November.

One notable difference in the winter of 2019 compared to the previous years is that, until October, newly polynya-produced ice flows westward only on the southern (coastal) side of the Central Grounded Icebergs. Also, through August, and most of September, icepack settles immediately adjacent to the northern section of the Iceberg Chain. This area is otherwise typically occupied by open polynya or polynya-produced ice. Both of these factors mean that the polynya-produced ice forms a narrower band closer to the coast. This is the case until October when ice becomes stuck to the south of the Central Grounded Icebergs causing the polynya-produced ice to divert around the northern side of the Central Grounded Icebergs.

In October and early November there are persistent polynya events and the new polynya-produced ice consistently moves westward, away from the polynya. By around 20 November there is an open polynya area without



substantial ice production across most of its area (Table 1). The polynya then extends to the west through November and December.

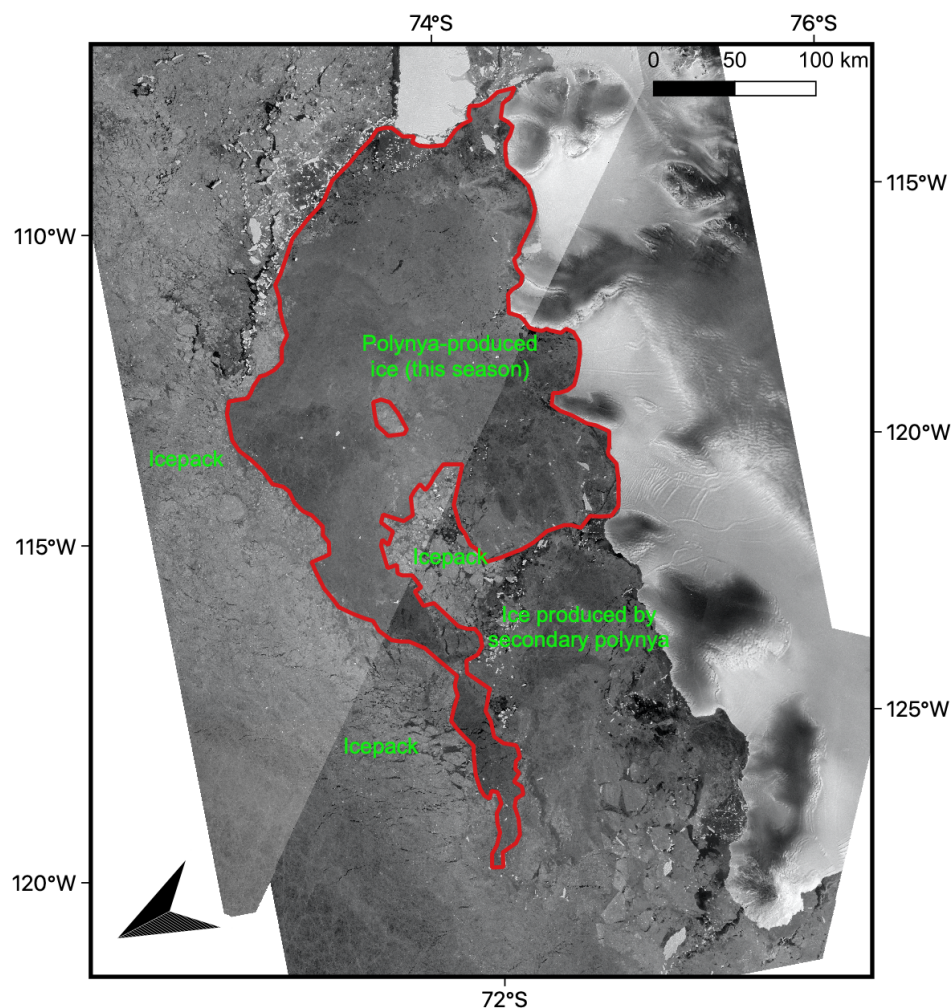


Fig. 3. Ice inside the red boundary is estimated, based on visual analysis of Video S1, to be approximately all the ice produced by the main polynya between 30 April and 4 November 2020. Sentinel-1 SAR image from 4 November 2020.

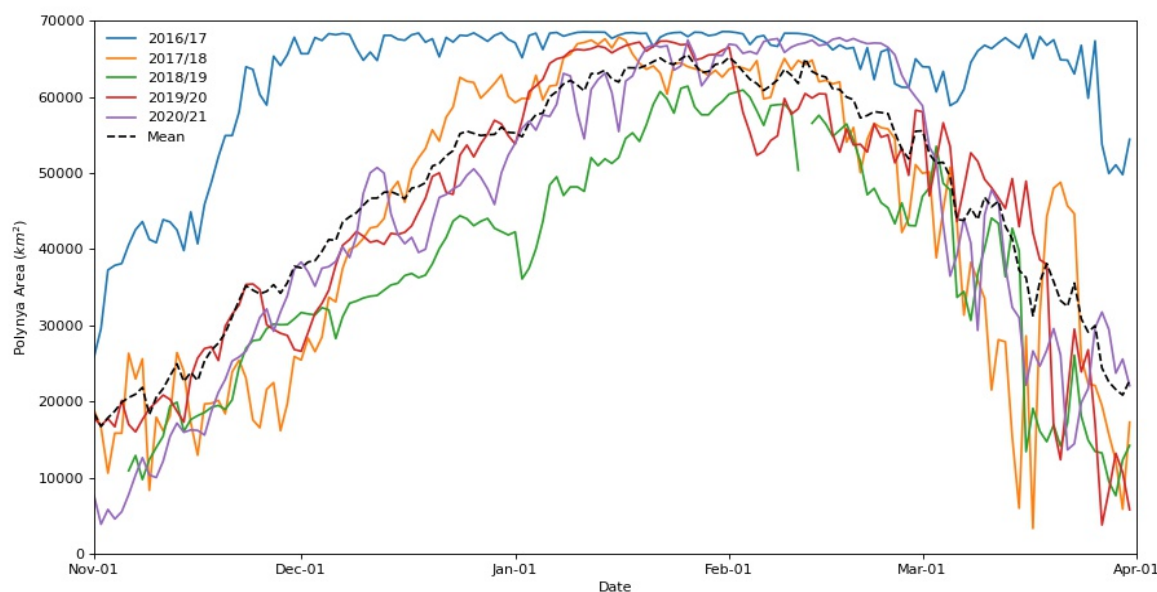
4.1.3 January 2020 - March 2021

As in the summer of 2018/19, throughout the summer of 2019/20 the polynya remains completely bound by icepack and isolated from the open ocean (Video S1). A more substantial area of icepack and fast ice lies between the ASP and the Pine Island Polynya, similar to the summer of 2017/18. Ice production is visibly taking place by early March and by 20 March 2020 new ice/ice-production is visible across the whole polynya (Table 1). Through



442 April-June, as in other years, regular polynya events originate from the Iceberg Chain and the Dotson Ice Shelf. In
443 late June icepack rounds the Iceberg Chain and pushes southward into the ASP, as happened in August-September
444 of 2019. There then follows a period largely lacking in imagery, but visual analysis of the polynya-produced ice in
445 the region-suggests that there is little ice production from then until early August. At this time the polynya-produced
446 ice that formed prior to 30 April has become stuck adjacent to the Central Grounded Icebergs, south and south-east
447 of the icebergs. This causes the new ice produced in the ASP from early August onwards to divert westward on the
448 north side of the Central Grounded Icebergs, entraining some fragments of the stuck, pre-August ice. From August
449 onwards, after some stuck ice becomes dislodged, a separate small ‘secondary polynya (Fig. 2a) also repeatedly
450 forms on the west side of the Central Iceberg Chain. New ice created by this small secondary polynya mixes with ice
451 formed by the main ASP and flows westward around Siple Island. Through November the polynya-produced ice
452 drifts away from the Iceberg Chain and Dotson Ice Shelf, and by 16 November ice production appears to have
453 mostly ceased (Table 1) as it enters the summer period. The summer polynya closes around 8 March 2021.

454 By analyzing Video S1 it is sometimes possible to visually track ice produced by particular polynya events
455 through the season. In particular, in 2020, with some uncertainty due to missing images, we are able to estimate that
456 approximately all of the ice produced between 30 April and 4 November by the main polynya (i.e. excluding the
457 secondary polynya located by the Central Grounded Icebergs) is contained within the red outline on 4 November in
458 Fig. 3. This section of polynya-produced ice totals 46452 km² in area.



459 **Fig. 4.** Daily summer (November-March) polynya area for each summer 2016/17-2020/21 (solid), and the daily
460 mean for the whole period (dashed).

461
462



4.2 Summer Polynya Area

In all years there is an overall increase in polynya area through November (Fig 4). On 1 November, the polynya has an area between 17 813 km² (2019) and 25 859 km² (2016). In the years 2017/18, 2018/19, 2019/20 and 2020/21 the polynya area then follows a similar pattern, but in 2016/17 it follows a distinct course. By 1 December in 2016 the polynya is open in approximately the whole ASP study area, with an area of 65 674 km², an increase of 154% from 1 November. In 2016/17 the polynya remains open across approximately the whole study area throughout December, January, and most of February and March, only beginning to significantly decline in late March (Fig 4) and into April (Fig 5). The polynya in 2016/17 maintains a higher area than in all other years throughout the whole summer, apart from a small period in late February when it is surpassed by 2020/21.

In 2017/18, 2018/19, 2020/21 and 2020/21 the polynya area has increased to between 25 439 km² (2017) and 38 310 km² (2020) by 1 December. From then the polynya continues to follow an overall increasing trend through December, with the polynya reaching its peak area in January in each of these years. In 2018/19 the peak area is substantially lower (61 113 km²) than in other years, and the polynya only maintains an area above 60 000 km² for six days in late January and early February. 2018/19 records the lowest area in comparison to other years on every day between 4 December and 3 February. In 2017/18, 2019/20 and 2020/21 the polynya behaves in a similar manner through most the period, with no one of those years consistently recording a higher area, and each year reaching a peak-open area that approximately fills the whole ASP study area. However, polynya area in 2020/21 reaches its peak later (January), and its decline begins later (late February). Notably, in 2017/18 the polynya experiences a temporary rapid re-opening as it increases from just 5 977 km² on 15 March to 48 779 km² on 21 March. This is an 82x increase in 6 days, and it is followed by a rapid decline. The polynya had the highest daily mean area for summer (November-March) in 2016/17, at 62 616 km², and 2018/19 had the lowest, at 38518 km². The mean daily area of 2017/18, 2019/20 and 2020/21 for summer was 44 013 km², 44 979 km² and 44 447 km², respectively.

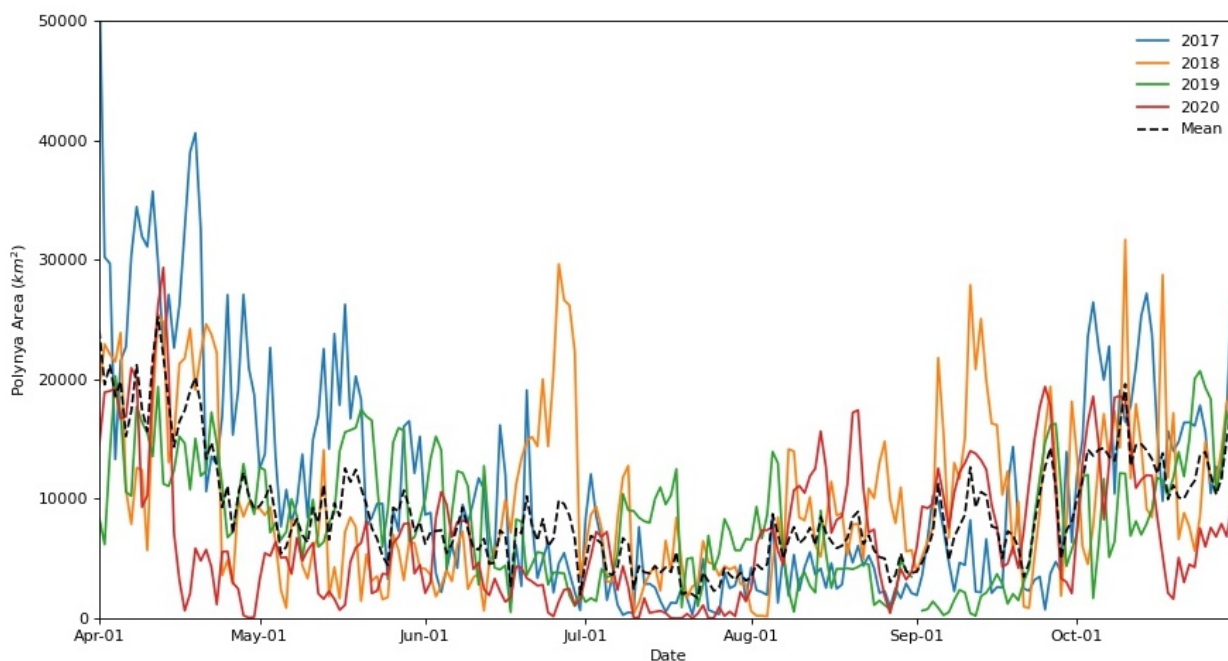


Fig. 5. Daily winter (April-October) polynya area for each winter 2017-2020 (solid), and the daily mean for the whole period, as measured from AMSR-2 SIC data (dashed).

4.3 Winter Polynya Area and Ice Production

In all years, polynya area exhibits an overall decline from the beginning of the winter period, when the polynya remains relatively large after the summer period (Fig. 5). This period, when the polynya remains relatively large but ice production has now begun, accounts for a substantial proportion of the annual ice production (Fig. 6; Fig. S2). On average, April/May accounts for 36% (39.6 km³) of annual ice production. The polynya then generally reaches a sustained winter low in area, where it fluctuates around and below 10 000 km². In 2020 the polynya area reaches its low in early April, while in 2017, 2019 and mean 2017-20 the area continues an overall decline through April, May and June. Polynya area and ice production then tend to remain low until an increase begins around September. In July polynya area remains below 10 000 km² in all years for the whole month apart from brief small fluctuations above this in 2018 and 2019. There are notable spikes in polynya area in the middle of the year, which are also exhibited in spikes in ice production. Most notably in June in 2018 polynya area spikes to 26 631 km². After a period of low polynya area, the area generally increases through September and October towards the summer period. In 2020 this period of area and ice production increase begins in August. This late-winter increase in polynya area is also exhibited in a corresponding marked increase in the rate of ice production. On average, September/October accounts for 42% (45.8 km³) of annual ice production.



We note that in 2017 between the dates of 1 April and 8 May a substantial portion of the calculated open polynya area, and ice production, occurs in the northwest of the ASP study area. This area is part of the open ocean and is separated by sea ice from the more-typically open polynya area adjacent to the iceberg chain. Typically ice-pack fills this northwest area, but in early 2017 it is open due to the lack of icepack in this sector in the summer of 2016/17, discussed in section 4.3 (Video S2; Fig. 11b).

Analysis of the spatial distribution of ice production across all years reveals that the mean daily ice production is highest in the area of the polynya adjacent to the Iceberg Chain, Thwaites Iceberg Tongue and Dotson Ice Shelf (Fig. 7). Mean annual ice production values (April-October) in this region surpass $17 \text{ m}^3/\text{m}^2$. Other notable areas of higher ice production lie along various parts of the coast and an area that corresponds to the secondary polynya by the Central Grounded Icebergs.

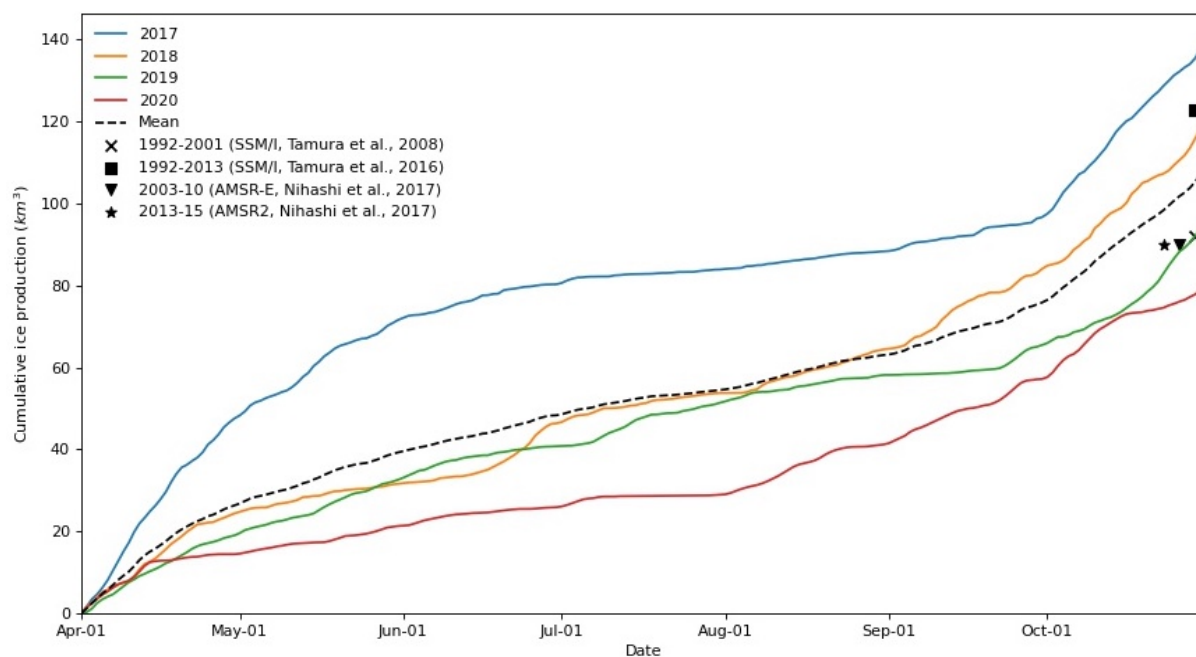


Fig. 6. Daily cumulative winter ice production for each winter (April-October) 2017-2020 (solid), and the mean for the period (dashed), as measured using heat-flux modeling of ERA-5 data and AMSR-2 SIC data. Also shown are mean annual measurements for 1992-2001 (Tamura et al., 2008), 1992-2013 (Tamura et al., 2016), 2003-10 and 2013-15 (Nihashi et al., 2017), along with the instrument used for each measurement. Note the previous studies' measurements covered the period March-October and used a study area that does not exactly correspond to ours.



Year	Mean Daily Polynya Area (km ²)	Total Annual Ice Production (km ³)	Total Mean Daily Ice Production (km ³)
2017	10 908 (9589)	139	0.67 (0.67)
2018	9 963 (7004)	121	0.57 (0.50)
2019	8 152 (5127)	95	0.45 (0.38)
2020	6 910 (5692)	80	0.38 (0.36)
Mean 2017-20	8 984 (7240)	109	0.52 (0.51)

Table 2. Estimates of Mean Daily Polynya Area, Total Annual Ice Production and Mean Daily Ice Production during the winters of 2017-2020, and for the daily mean of the period. Numbers in brackets indicate the standard deviation.

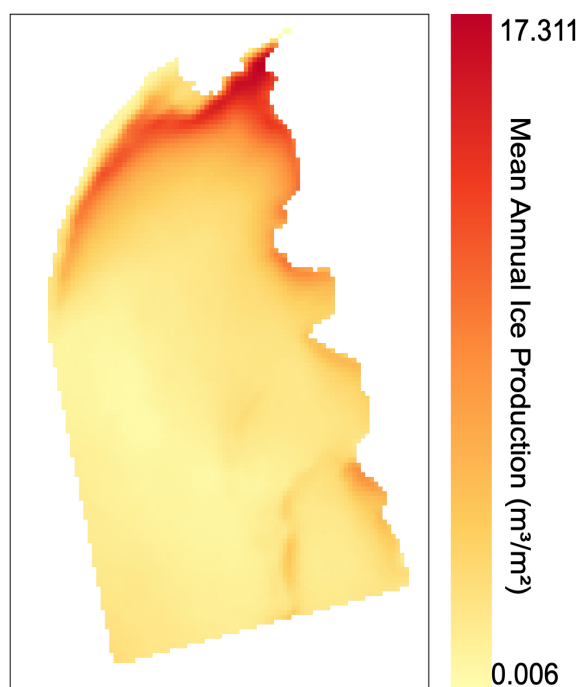


Fig. 7. Mean Annual Ice Production for all winter study periods (April-October 2017-2020). The region corresponds to the region within the green outline in Fig. 1b



4.4 Wind and polynya area

Daily mean wind speed at the polynya site and polynya area during the winter period has a weak but significant positive correlation (0.33, $P < 0.05$) (Fig. 8). Many day-to-day variations in polynya area are not correlated with wind speed, however it is clear that notable spikes in polynya area do often occur on days with high wind speed (Fig. S3). For example, the three highest polynya areas recorded in 2020 after April all occur alongside the three highest spikes in wind speed post-April. By viewing the mean spatial distribution of wind it is clear that the ASP forms in an area of relatively high winds (Fig. 9). A band of high winds with a mean speed of around 8 - 9 ms^{-1} exists along the coast from Thwaites Glacier, over the Thwaites Iceberg Tongue and into the eastern area of the ASP study area, where the main polynya originates.

The mean wind direction throughout the ASP study area is approximately southerly. While this direction corresponds to the direction in which the polynya sometimes forms northward off the Dotson Ice Shelf, it does not correspond to the more typical westward formation off the iceberg chain.

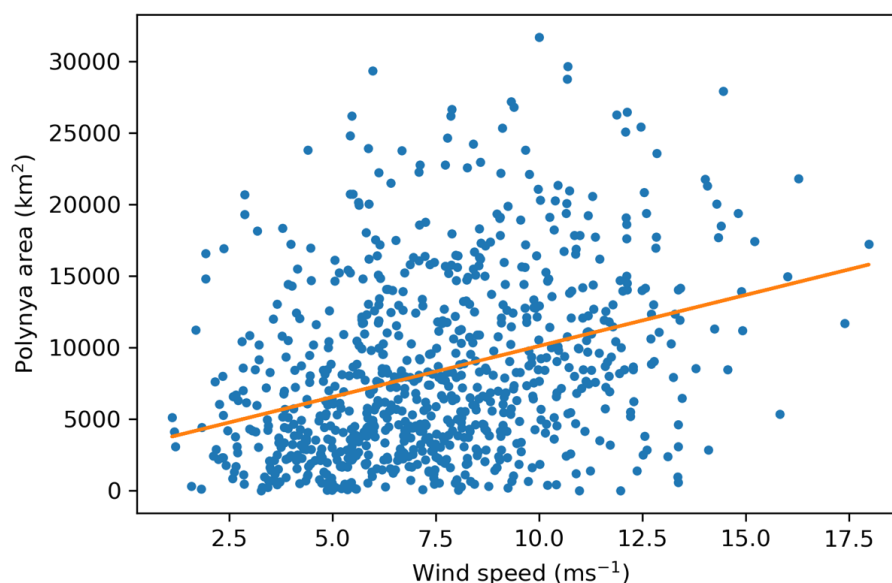
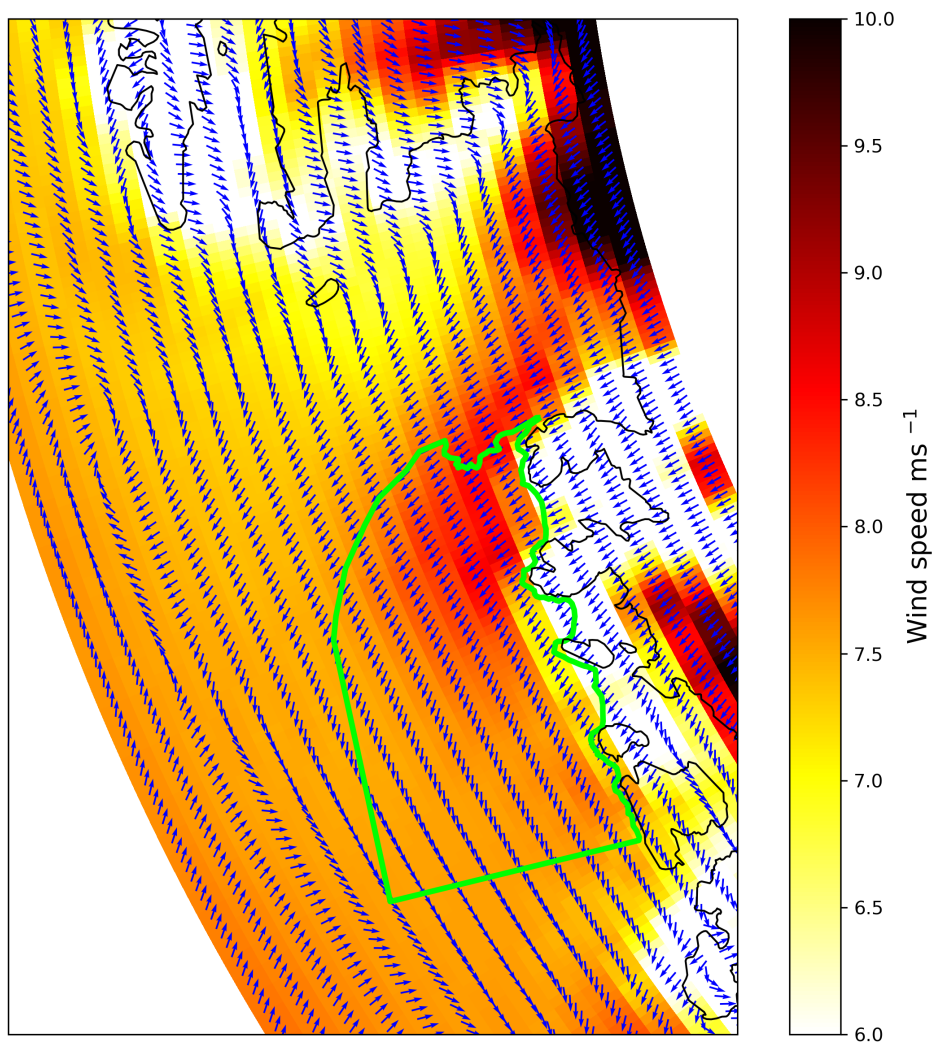


Fig. 8. Scatter plot of daily polynya area and wind speed for all winter days (April-October 2017-2020), except for the period 1 April - 8 May 2017 (which is excluded because during this time the study site included a substantial open area on the seaward side of icepack and at a distance from the area used to calculate wind speed (Fig. 11b)). The Pearson Product Correlation Coefficient is 0.33 ($P < 0.05$).



540 **Fig. 9.** Mean wind speed and direction for the period 1 November 2016 to 31 December 2020. The green box repre-
 541 sents the ASP study area, the same as the green box in Fig 1b. Daily wind speed and direction is included as Video
 542 S3.

543

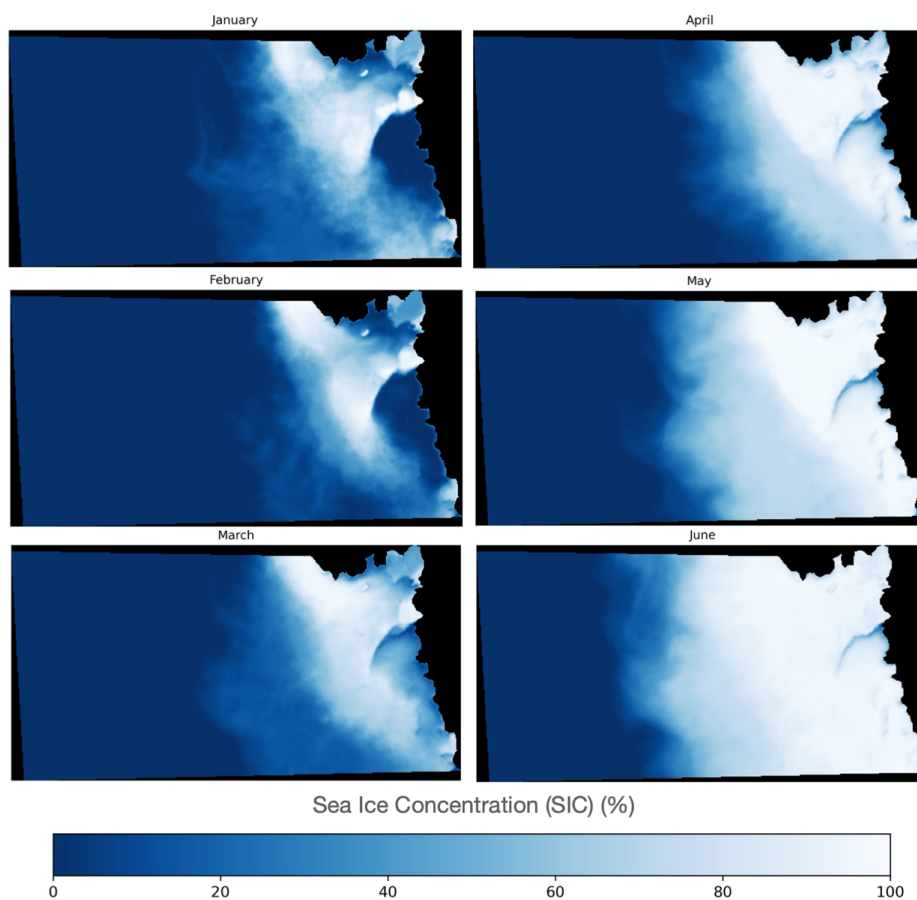
544

545

546



547



548
 549
 550
 551
 552
 553
 554
 555
 556
 557
 558
 559
 560
 561

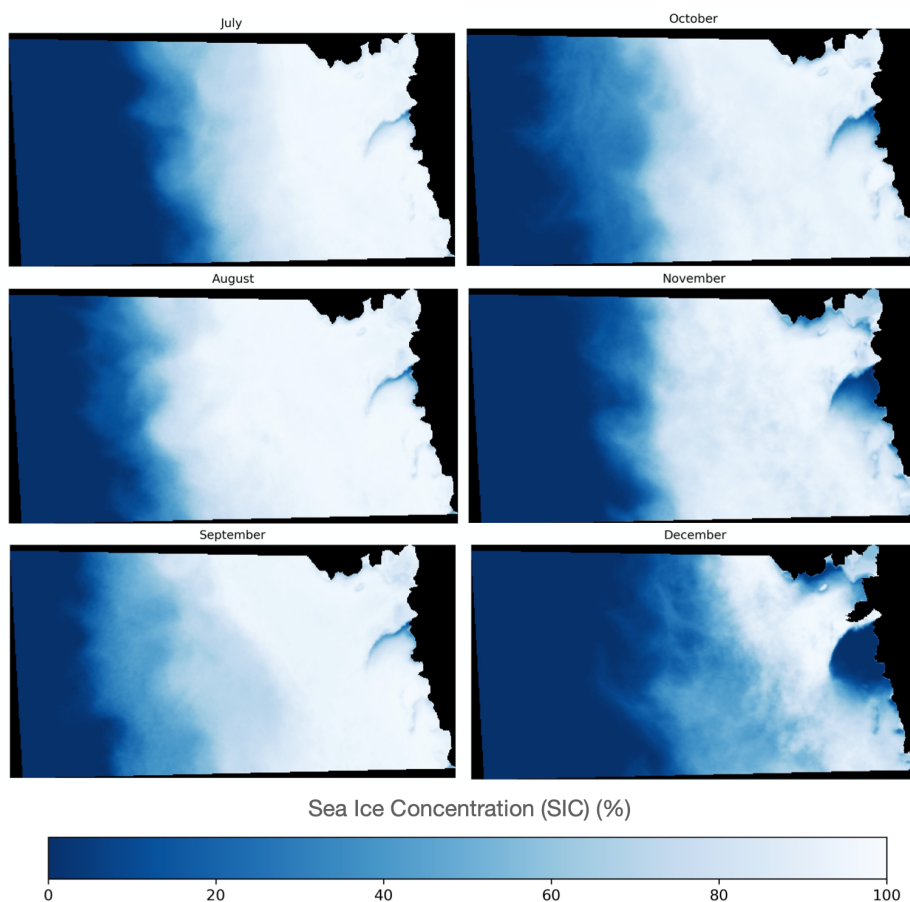


Fig. 10. Mean monthly SIC for the broader ASP region for the period November 2016 to March 2021. The area corresponds to that shown by red box in Fig. 1a. Daily data is shown in Video S2.

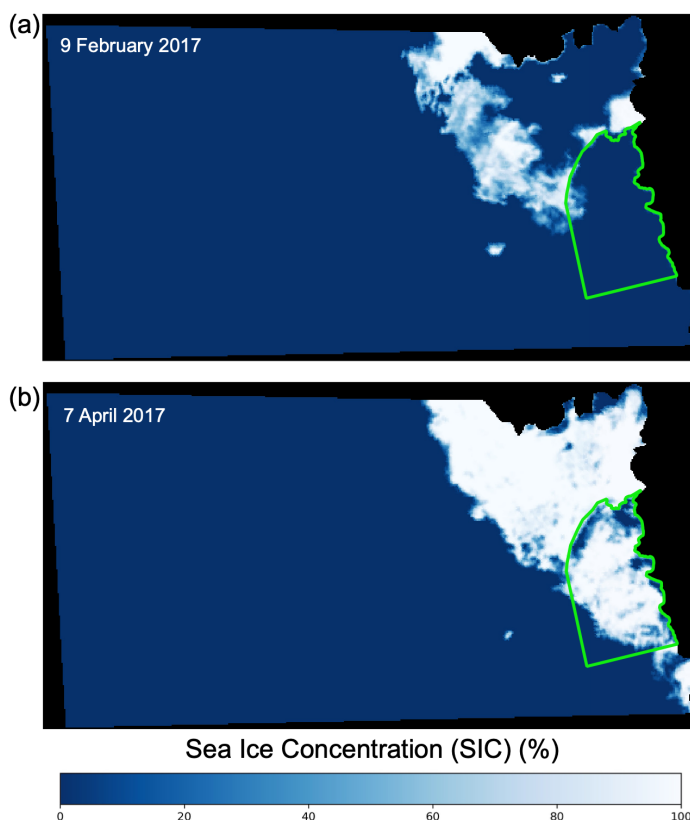


Fig. 11. SIC for the broader ASP region on two days in 2017, during and following a summer of record-low SIC. The area corresponds to that shown by red box in Fig. 1a.

4.5 Broader SIC

Analysis of the SIC over a broader area also shows daily changes in the polynya area and how it relates to changes in the icepack. The mean monthly cycle of the polynya can be seen in Fig. 10 and presents a similar picture of the polynya as described in sections 4.1- 4.3. The broader icepack has a minimum total SIC of 1 975 921 in January and remains similar in February. From March the broader icepack can be seen to expand in area as the polynya begins to close and continues to increase until a peak of 6 588 615 cumulative SIC in September. From October the icepack begins a marked decline into summer. Interannual variation can be seen in Fig. S4 and Video S2, with maximum icepack area occurring in August or September each year, and minimum icepack in January or February.

During the summer of 2016/17 the icepack is notably sparse (Fig. 11; S4). Around 29 December 2016 a gap in the icepack connects the ASP to the open ocean to north. The icepack continues to diminish and the gap connecting the ASP to the open ocean broadens until by February the polynya is only bound by part of the Iceberg Chain and Thwaites Iceberg Tongue. The total SIC reaches a minimum of 421 434 on 5 February 2017, 35% of the next lowest annual minimum (2019/20). Gaps in icepack around the Iceberg Chain mean that the ASP has essentially joined with the Pine Island Polynya through the Iceberg Chain for a period in this year. The narrow band of



icepack from the east closes the polynya off again in March but the band of adjacent icepack remains so narrow that, as mentioned, there is open ocean inside our ASP study area until 9 May (Video S2).

5. Discussion

Our analysis shows that in some ways the ASP, between November 2016 and March 2021, behaves as is typical for Antarctic coastal polynyas. During the summer the polynya becomes larger and remains ice-free (Fig. 4, Video S1), while during the winter it becomes smaller, opening up during ice-producing polynya ‘events’ (Figs. 5-6, Video S1). These polynya events and changes in polynya area can sometimes be attributed to higher wind speeds (Figs 8-9, S3).

Our qualitative analysis of Sentinel-1 SAR imagery, however, also reveals distinct characteristics of the ASP which are not possible to decipher from sea ice concentration data, other quantitative methods, or indirect observation. First, we note that while in many other polynyas, such as the Ross Ice Shelf Polynya, new polynya-produced ice is typically efficiently evacuated away from its origin (Dai et al., 2020), this is not the case at the ASP. Instead, ice formed by the ASP often remains in the ASP study area for months (Video S1, Fig. 3). In fact, this polynya-produced ice does not consistently flow in a direction away from the polynya. While its overall direction is westward, away from the polynya, the ice ‘heaves’ and temporarily flows ‘backward’ (‘back-fills’), as has also been observed at the Mertz Glacier Polynya (Massom et al., 2017). The ice also gets ‘stuck’ in the region, particularly around grounded icebergs, which are grounded in areas where there are topographic highs in the sea floor (Fig. 2a, e).

The tendency of ice produced by the ASP to remain in the vicinity of the polynya for prolonged periods, become stuck, and sometimes flow back eastward towards the site of its formation, influences the polynya and ice production in two key ways. First, when ice moves eastward while the polynya is open it contributes to the closure of the polynya, and thus the cessation of ice production. Typically it is assumed that an open polynya during winter closes due to new ice production (e.g. Cheng et al., 2017). However, the ASP may close both due to ice production and movement of previously-produced ice into the polynya. Second, we suggest that the blockages of ice in the vicinity of the polynya reduce the size and frequency of polynya events by hindering the ability of ice to move out of the polynya and open it up. Again, by reducing the size and duration of open polynya area during winter, ice production is limited.

We also note that the ASP forms along the coast westward off a chain of icebergs that extend from the Thwaites Iceberg Tongue. While some polynyas, such as the Ross Ice Shelf polynya, form off and away from the coast, the majority of Antarctic polynyas have been shown to form westward off glacier ice tongues or protruding fast ice (Nihashi et al., 2017). In the case of the ASP, its location and orientation is determined by the presence of the ‘Iceberg Chain’, which is in turn determined by the presence of a bathymetric high (Figs. 1-2). Stammerjohn et al. (2015) refer to the polynya as forming off a ‘fast ice tongue’ but we prefer to refer to the ‘Iceberg Chain’ as the eastern boundary. While a section of fast ice exists amongst, and adjacent to, a section of the southern part of the Iceberg Chain, the extent of this fast ice varies and it only ever extends along a portion of the Iceberg Chain. The Iceberg Chain remains virtually the same length throughout our observations. The polynya consistently forms off the



Iceberg Chain regardless of the state or extent of the fast ice. This means that, unlike polynyas that form off variable fast ice (Nihashi et al., 2017), the fundamental morphology of the ASP remains stable through the period and is likely to remain so. We also note that at no point do we observe significant portions of icepack to ‘break through’ the Iceberg Chain from east, regardless of the state of fast ice extent or conditions, and thus the icebergs and the bathymetric high persistently ‘shield’ the polynya from icepack inflow.

Another notable feature of the ASP is the development of a ‘secondary polynya’ during the winter (Fig. 2a), where ice production also takes place. This is a polynya that forms within the ASP study area, in an area that is usually part of main ASP during the summer, but it is not typically congruent with the ‘main’ polynya during the winter. The polynya forms at the site of the ‘Central Grounded Icebergs’ and associated ‘stuck’, transient fast ice. Because some ice has become stuck over the bathymetric high, when adjacent ice drifts away, a polynya opens. This feature again highlights the significance of the bathymetry of the region for sea ice production and dynamics.

In line with previous studies of the ASP we find that the ASP is an important site of ice production throughout the winter. Our estimates of annual ice production for 2019 and the mean for 2017-20 fall within the range of predictions by Tamura et al. (2008; 2016) and Ohshima et al. (2017) for 1992-2001/2003-10/2013-15 (90 - 117 km³) (Fig. 6). Our estimates for total annual ice production for 2017 (139 km³) and 2018 (121 km³) are higher than the highest estimate of those studies, while for 2020 (80 km³) it is lower. This suggests no significant trend in interannual ice production can be discerned from comparing the period of our study to these previous studies. Some caution must be used in this comparison, however, because those studies include March in ice production calculations and our ASP study area does not exactly correspond to theirs.

We find that the shoulder seasons of April/May and September/October are particularly important for ice production due to the higher polynya area at these times, accounting for 36% and 42% of the annual ice production, respectively. This is particularly the case in 2017, when an exceptionally high open polynya area in the summer, due to low icepack conditions (discussed below), continues into the winter period (Figs. 4-6). However, we show that at least some polynya area opens and some ice production occurs throughout the whole winter (Fig. 5-6). Additionally there can be spikes in polynya area and ice production in the deepest winter months. Most notably, polynya area reaches 26 631 km² in June. Such isolated, winter events are not reflected in the daily mean for the whole study period, but only when analyzing daily changes for each year (Fig. 5), highlighting the importance of analyzing polynya area and ice production at the daily scale to discern important polynya dynamics.

When comparing our results to those of Cheng et al. (2017), who used the same method for calculating ice production at the Ross Ice Shelf Polynya, we find that the ASP produces substantially less ice. Between 2003 and 2015 they found ice production for the Ross Ice Shelf Polynya was between 164 and 313 km³ (also for April - October) compared to 80 to 139 km³ (this study). This is in line with other studies that compare the two polynyas (Tamura et al. 2008; 2016; Nihashi et al. 2017). We suggest that one limit on polynya area and ice production for the ASP compared to the larger Ross Ice Shelf Polynya, is that the ASP typically forms off the Iceberg Chain. The Iceberg Chain has a stable length of ~190 km, limited by the length of the seafloor sill on which it is grounded, and is an upper limit on the polynya in one dimension. The Ross Ice Shelf Polynya, on the other hand, forms off a coast-



line, and is only typically limited in this spatial dimension by weather/oceanographic conditions. Another comparative limit on the ASP's ice production is the previously discussed tendency for polynya-produced ice to inhibit further opening of the polynya due to blockages and reversals in ice drift. This process could also partly explain why Cheng et al. (2017) found ice production to remain relatively consistent throughout the winter for the Ross Ice Shelf Polynya, whereas we find ice production for the ASP in June-August to be much lower than in the shoulder months of April/May and September/October.

We also note the polynya-produced ice leaves our study area and enters the adjacent sector of the Amundsen Sea to the west, rather than traveling away from the coast after formation. This westward flow of the ice away from the polynya is likely, in this section, primarily due to the prevalence of westward ocean currents in the region (St-Laurent et al., 2019), rather than wind which has a mean southerly direction (Fig. 7). These ocean currents have been shown to carry icebergs away from our study region, westward through the Amundsen Sea and into the Ross Sea (Koo et al., in review). Broader prevailing easterly winds likely play a dominant role in sea ice produced by the ASP eventually drifting to the Ross Sea, as part of a coastal band of westward ice drift (Assmann et al., 2005). The fact that the polynya-produced ice remains by the coast may also be influenced by the inflow of older, thicker icepack into our study area. Icepack appears to flow into the region from the Bellingshausen Sea (Video S1, S2) and flows parallel to the ASP-produced ice, potentially playing some role in 'trapping' the ice by the coast. The westward flow of the ice suggests that the level of ice production in the ASP is significant for the adjacent sector of the Amundsen Sea and the Ross Sea.

During the summer we observe the ASP to behave in a similar way in 2016/17 - 2020/21 as Stammerjohn et al. (2015) showed for the period 1979 - 2014. As they did, we find the polynya to open every summer during our study period. We do not note any shift in the location of opening, with the location remaining in the same place as Stammerjohn et al. (2015) noted that it had shifted to in 1992/93. As they did for the years 1992, 1993, 1995, 1997, 2003, and 2010, we also note that in 2016/17, there is no icepack adjacent to the ASP in the north and west. This is due to limited advection from the Bellingshausen Sea and Pine Island Polynya, and it causes the ASP to become congruent with the open ocean (Fig. 11). This year was noted as a year of unprecedented springtime retreat and low sea ice concentration for Antarctic sea ice, and was associated with a series of record atmospheric circulation anomalies and sea surface temperatures (Turner et al., 2017). These broader sea ice conditions caused the polynya to be open in approximately the whole ASP study area through most of the summer in 2016/17, from late November to March. During this time there is also little-to-no distinction between the ASP and the neighboring Pine Island Polynya, other than the presence of the Iceberg Chain (Fig. 11a, Video S1). The effect of these extraordinary sea ice conditions in 2016/17 on the polynya in summer, and early winter as mentioned above, may offer insight into how the ASP will behave more commonly in future if climate change makes such conditions more likely.

We note that while Stammerjohn et al. (2015) found the largest polynya area to be February in all but two years during 1979 - 2014, we find the polynya area to be highest in January in each year apart from 2016/17 (when it reaches the peak in November) (Fig. 4). Arrigo et al. (2012) also generally found the polynya area to increase until a later peak in February for the years 1997/98 - 2009/10. While there should be some caution in directly comparing our results with those, due to varying datasets, methods and definitions of the study area, we suggest that a shift in



the timing of maximum summer area would promote primary productivity in the polynya. Arrigo et al. (2012) found primary productivity (per unit area) to typically peak in January, and to be declining by the time of the polynya area peak. If the polynya reaches a higher area at an earlier time, when primary productivity is higher, we suggest the potential for primary productivity may be larger during our study period.

6. Conclusions

Focusing on the summers of 2016/17 - 2020/21 and the winters of 2017 - 2020, we present the first detailed study of year-round variations in the Amundsen Sea Polynya's behavior, area, and ice production. In particular, we take advantage of the recent availability of Sentinel-1 SAR imagery to qualitatively assess the dynamics of the polynya through the whole year.

Our findings agree with previous studies of earlier periods in finding that the ASP produces a substantial amount of ice through the winter, with some inter-annual variation. We add that the shoulder seasons of April/May and September/October dominate winter ice production, contributing a combined 78%. However, large polynya events, often associated with high winds, can occur throughout the winter, promoting significant ice production.

The ASP opens each summer in November and closes in March or early April, with peak area typically occurring in January. We find that broader regional sea ice conditions can play an important role in the polynya in summer, with the record-low sea ice extent in 2016/17 causing the ASP to become part of the open ocean to the north and join with the Pine Island Polynya to the east.

Through our qualitative assessment we identify that the ASP behaves in a distinct manner. The polynya typically forms in a westward direction off a persistent chain of grounded icebergs that are grounded along a bathymetric high. Ice produced by the polynya is not efficiently evacuated from the site as with other polynyas such as the Ross Ice Shelf Polynya. Instead it stays within the study site, typically for months through the winter, sometimes becoming stuck. This behavior is related to local topographic sea-floor highs which cause icebergs to become grounded and ice to become stuck. At times another smaller 'secondary polynya' forms within the study area adjacent to grounded icebergs. Relatedly, ice produced by the polynya does not consistently move away from the ASP, instead 'heaving' and sometimes drifting back towards it, contributing to its closure and limiting ice production. Unlike some other polynyas, the polynya-produced ice also drifts westward into other sectors, instead of north, away from the coast. These behaviors should be accounted for when considering the ASP's influence on the region's sea ice, biology and oceanography.

Given temporal and spatial gaps in Sentinel-1 SAR's coverage, we do not find that it can replace passive microwave or sea ice concentration datasets for analyzing daily changes in polynya area or ice production. However, we find that the ability to directly observe and qualitatively analyze the polynya at a high spatial and temporal resolution, year-round, with Sentinel-1 imagery provides important insights that are not possible with those other datasets. We also note that it is sometimes possible to visually-track ice created by particular polynya events for several months as it drifts. Employing ice-tracking algorithms to track ice produced by polynya events in Sentinel-1 images, with measurements of ice thickness (e.g. from satellite altimetry), could help further quantify ice production by polynyas and extract more potential from Sentinel-1 datasets.



739 *Code and Data Availability*

740 Code for data processing and production of figures and videos is available at
 741 <https://github.com/geogeordie/AmundsenSeaPolynyaPaper>. All processing was done with freely available software,
 742 and all data is freely available. Sentinel-1 images were processed in Google Earth Engine or downloaded from:
 743 asf.alaska.edu. BedMachine Antarctica V2 was downloaded from: <https://nsidc.org/data/nsidc-0756>. Sea ice concen-
 744 tration data was downloaded from: <http://seaice.uni-bremen.de/>. ERA5 climate data was downloaded from:
 745 <https://cds.climate.copernicus.eu>. The MODIS image used for Fig. 1b was downloaded from:
 746 <https://worldview.earthdata.nasa.gov/>

748 *Video Supplement*

749 Video S1: <https://doi.org/10.5281/zenodo.5179444>
 750 Video S2: <https://doi.org/10.5281/zenodo.5179509>
 751 Video S3: <https://doi.org/10.5281/zenodo.5179590>

753 *Author Contributions*

754 GJM primarily conceived the study, processed and analyzed all data and produced all figures. SFA and AMM-N
 755 also contributed to the design of the study and all authors discussed the results and were involved in editing the man-
 756 uscript.

758 *Competing Interests*

759 The authors declare that they have no conflict of interest.

761 *Financial Support*

762 This work was supported by NASA grant #80NSSC19M0194.

764 *Acknowledgements*

765 We gratefully acknowledge the European Space Agency for making available Sentinel-1 data and the SNAP
 766 toolbox, and Google Earth Engine for hosting and processing Sentinel-1 data. We acknowledge the free package
 767 Quantarctica, developed by the Norwegian Polar Institute, for use in Fig. 1a. We thank the University of Bremen
 768 Sea Ice Remote Sensing Group for processing and making available their sea ice concentration product and the Japa-
 769 nese Space Exploration Agency for launching and managing AMSR2. We also acknowledge the ECMWF, NSIDC
 770 and NASA for freely-available data. Among others, the free, open-source software packages QGIS, GDAL, Python,
 771 NumPy and Matplotlib were invaluable in this research. We also thank the GIS and StackOverflow StackExchange
 772 communities for resources that aided data processing.

774 **References**

775 Armstrong, T.: World meteorological organization: WMO sea-ice nomenclature. Terminology, codes and illustrated
 776 glossary. J. Glaciol., 11, 148–149. <https://doi.org/10.3189/S0022143000022577>, 1972.



- 777
778 Arrigo, K. R., van Dijken, G. L., and Bushinsky, S.: Primary production in the Southern Ocean, 1997–2006, J. Geophys. Res., 113, C08004. <https://doi.org/10.1029/2007JC004551>, 2008a.
- 779
780
781 Arrigo, K. R., van Dijken, G. L., and Long, M.: Coastal Southern Ocean: A strong anthropogenic CO₂ sink. Geophys. Res. Lett., 35, L21602. <https://doi.org/10.1029/2008GL035624>, 2008b.
- 782
783
784 Arrigo, K. R., Lowry, K. E., and van Dijken, G. L.: Annual changes in sea ice and phytoplankton in polynyas of the Amundsen Sea, Antarctica. Deep Sea Research, II 71–76: 5–15. <https://doi.org/10.1016/j.dsr2.2012.03.006>, 2012.
- 785
786
787 Arrigo, K. R. and van Dijken, G. L.: Phytoplankton dynamics within 37 Antarctic coastal polynya systems. J. Geophys. Res., 108, 3271 <https://doi.org/10.1029/2002jc001739>, 2003.
- 788
789
790 Arthur, J. F., Stokes, C. R., Jamieson, S. S. R., Miles, B. W. J., Carr, J. R., and Leeson, A. A.: The triggers of the disaggregation of Vovaykov Ice Shelf (2007), Wilkes Land, East Antarctica, and its subsequent evolution. J. Glaciol <https://doi.org/10.1017/jog.2021.45>, 2021.
- 791
792
793
794 Assmann, K. M., Hellmer, H. H., and Jacobs, S. S.: Amundsen Sea ice production and transport. J. Geophys. Res., 110, C12013. <https://doi.org/10.1029/2004JC002797>, 2005.
- 795
796
797 Banwell, A. F., Willis, I. C., Macdonald, G. J., Goodsell, B., Mayer, D. P., Powell, A., and MacAyeal, D. R.: Calving and rifting on the McMurdo Ice Shelf, Antarctica. Ann. Glaciol., 58, 78–87. <https://doi.org/10.1017/aog.2017.12>, 2017.
- 798
799
800
801 Bett, D. T., Holland, P. R., Naveira Garabato, A. C., Jenkins, A., Dutrieux, P., Kimura, S., and Fleming, A.: The impact of the Amundsen Sea freshwater balance on ocean melting of the West Antarctic Ice Sheet. J. Geophys. Res.: Oceans, 125, e2020JC016305. <https://doi.org/10.1029/2020JC016305>, 2020.
- 802
803
804
805 Bracegirdle, T. J.: Climatology and recent increase of westerly winds over the Amundsen Sea derived from six reanalyses. Int. J. Climatol., 33, 843–851. <https://doi.org/10.1002/joc.3473>, 2013.
- 806
807
808 Bromwich, D. H. and Kurtz, D. D.: Katabatic wind forcing of the Terra Nova Bay polynya. J. Geophys. Res., 89, 3561. <https://doi.org/10.1029/JC089iC03p03561>, 1984.
- 809
810
811 Bromwich, D., Liu, Z., Rogers, A. N., and Van Woert, M. L.: Winter atmospheric forcing of the Ross Sea polynya. Ocean ICE Atmos. Int. Antarct. Cont. Margin, 75, 101–133. <https://doi.org/10.1029/AR075p0101>, 1998.
- 812
813
814 Bromwich, D. H., Carrasco, J. F., Liu, Z., and Tzeng, R. Y.: Hemispheric atmospheric variations and oceanographic impacts associated with katabatic surges across the Ross ice shelf, Antarctica. J. Geophys. Res.-Atmos, 98, 13045–13062. <https://doi.org/10.1029/93JD00562>, 1993.
- 815
816
817
818 Cheng, Z., Pang, X., Zhao, X., and Tan, C.: Spatio-Temporal Variability and Model Parameter Sensitivity Analysis of Ice Production in Ross Ice Shelf Polynya from 2003 to 2015. Remote Sensing, 9, 934. <https://doi.org/10.3390/rs9090934>, 2017.
- 819
820
821
822 Cheng, Z., Pang, X., Zhao, X., and Stein, A.: Heat Flux Sources Analysis to the Ross Ice Shelf Polynya Ice Production Time Series and the Impact of Wind Forcing, Remote Sensing, 11, 188. <https://doi.org/10.3390/rs11020188>, 2019.
- 823
824
825
826 Dai, L., Xie, H., Ackley, S. F., and Mestas-Núñez, A. M.: Ice Production in Ross Ice Shelf Polynyas during 2017–2018 from Sentinel-1 SAR Images. Remote Sensing, 12, 1484. <https://doi.org/10.3390/rs12091484>, 2020.
- 827
828
829 Drucker, R., Martin, S., and Kwok, R.: Sea ice production and export from coastal polynyas in the Weddell and Ross Seas. Geophys. Res. Lett., 38, L1705. <https://doi.org/10.1029/2011GL048668>, 2011.
- 830
831
832 Greene, C. E., Young, D. A., Gwyther, D. E., Galton-Fenzi, B. E., and Blankenship, D. D.: Seasonal dynamics of



- 833 Totten Ice Shelf controlled by sea ice buttressing. *Cryosphere*, 12, 2869–2882. [https://doi.org/10.5194/tc-12-2869-](https://doi.org/10.5194/tc-12-2869-2018)
834 [2018](https://doi.org/10.5194/tc-12-2869-2018), 2018.
- 835
- 836 Grossmann, S. and Dieckmann, G. S.: Bacterial Standing Stock, Activity, and Carbon Production during Formation
837 and Growth of Sea–Ice in the Weddell Sea, Antarctica. *Appl. Environ. Microb.*, 60, 2746–2753.
838 <https://doi.org/10.1128/aem.60.8.2746-2753.1994>, 1994.
- 839
- 840 Hersbach, H., Bell, B., Berrisford, P., Biavati, G., Horányi, A., Muñoz Sabater, J., Nicolas, J., Peubey, C., Radu, R.,
841 Rozum, I., Schepers, D., Simmons, A., Soci, C., Dee, D., and Thépaut, J.-N.: ERA5 monthly averaged data on single
842 levels from 1979 to present. Copernicus Climate Change Service (C3S) Climate Data Store (CDS). (Accessed on <
843 01-04-2021), <https://doi.org/10.24381/cds.fl7050d7>, 2019.
- 844
- 845 IMBIE team: Mass balance of the Antarctic ice sheet from 1992 to 2017. *Nature* 558, 219–222.
846 <https://doi.org/10.1038/s41586-018-0179-y>, 2018.
- 847
- 848 Ito, M., Ohshima, K. I., Fukamachi, Y., Mizuta, G., Kusumoto, Y., and Nishioka, J.: Observations of frazil ice for-
849 mation and upward sediment transport in the Sea of Okhotsk: A possible mechanism of iron supply to sea ice. *J. Ge-*
850 *ophys. Res.–Oceans*, 122, 788–802. <https://doi.org/10.1002/2016JC012198>, 2017.
- 851
- 852 Kimura, N. and Wakatsuchi, M.: Increase and decrease of sea ice area in the Sea of Okhotsk: Ice production in
853 coastal polynyas and dynamic thickening in convergence zones. *J. Geophys. Res.–Oceans*, 109, C09S03.
854 <https://doi.org/10.1029/2003JC001901>, 2004.
- 855
- 856 Kitade, Y., Shimada, K., Tamura, T., Williams, G. D., Aoki, S., Fukamachi, Y., Roquet, F., Hindell, M., Ushio, S.,
857 and Ohshima, K. I.: Antarctic Bottom Water production from the Vincennes Bay Polynya, East Antarctica. *Ge-*
858 *ophys. Res. Lett.*, 41, 3528–3534. <https://doi.org/10.1002/2014GL059971>, 2014.
- 859
- 860 Koo, Y., Xie, H., Ackley, S. F., Mestas-Núñez, A. M., Macdonald, G. J., and Hyun, C.-U.: Semi-automated tracking
861 of iceberg B43 using Sentinel-1 SAR images via Google Earth Engine. *Cryosphere Discuss.*,
862 <https://doi.org/10.5194/tc-2021-131>, 2021 [in review]
- 863
- 864 Krumpen, T., Hölemann, J. A., Willmes, S., Morales Maqueda, M. A., Busche, T., Dmitrenko, I. A., Gerdes, R.,
865 Haas, C., Heinemann, G., Hendricks, S., Kassens, H., Rabenstein, L., and Schröder, D.: Sea ice production and wa-
866 ter mass modification in the eastern Laptev Sea. *J. Geophys. Res.–Oceans*, 116, C05014.
867 <https://doi.org/10.1029/2010JC006545>, 2011.
- 868
- 869 Marzocchi, A. and Jansen, M. F.: Global cooling linked to increased glacial carbon storage via changes in Antarctic
870 sea ice, *Nat. Geosci.*, 12, 1001–1005. <https://doi.org/10.1038/s41561-019-0466-8>, 2019.
- 871
- 872 Massom, R. A., Hill, K. L., Lytle, V. I., Worby, A. P., Paget, M. J., and Allison, I.: Effects of regional fast-ice and
873 iceberg distributions on the behaviour of the Mertz Glacier polynya, East Antarctica. *Ann. Glaciol.*, 33, 391–398.
874 <https://doi.org/10.3189/172756401781818518>, 2001.
- 875
- 876 Massom, R. A., Scambos, T. A., Bennetts, L. G., Reid, P., Squire, V. A., and Stammerjohn, S. E.: Antarctic ice shelf
877 disintegration triggered by sea ice loss and ocean swell. *Nature*, 558, 383–389. [https://doi.org/10.1038/s41586-018-](https://doi.org/10.1038/s41586-018-0212-1)
878 [0212-1](https://doi.org/10.1038/s41586-018-0212-1), 2018.
- 879
- 880 Matsuoka, K., Skoglund, A., Roth, G., de Pomereu, J., Griffiths, H., Headland, R., Herried, B., Katsumata, K., Le
881 Brocq, A., Licht, K., Morgan, F., Neff, P. D., Ritz, C., Scheinert, M., Tamura, T., Van de Putte, A., van den Broeke,
882 M., von Deschanden, A., Deschamps-Berger, C., Van Liefferinge, B., Tronstad, S., and Melvær, Y.: Quantarctica,
883 an integrated mapping environment for Antarctica, the Southern Ocean, and sub-Antarctic islands. *Environ. Modell.*
884 *Softw.*, 140, 105015. <https://doi.org/10.1016/j.envsoft.2021.105015>, 2021.
- 885
- 886 Morales Maqueda, M. A., Willmott, A. J., and Biggs, N. R. T.: Polynya dynamics: a review of observations and
887 modeling. *Review of Geophysics*, 42, RG1004. <https://doi.org/10.1029/2002RG000116>, 2004.
- 888



- Morelli, S. and Parmiggiani, F.: Wind over Terra Nova Bay (Antarctica) during a polynya event: Eta model simulations and satellite microwave observations. *Eur. Phys. J. Plus* 128, 135 (2013). <https://doi.org/10.1140/epjp/i2013-13135-8>, 2013.
- Morlighem, M.: MEaSUREs BedMachine Antarctica, Version 2. Boulder, Colorado USA. NASA National Snow and Ice Data Center Distributed Active Archive Center. <https://doi.org/10.5067/C2GFER6PTOS4>, 2019. [Date Accessed: 01-04-2021].
- Nihashi, S., and Ohshima, K. I.: Circumpolar Mapping of Antarctic Coastal Polynyas and Landfast Sea Ice: Relationship and Variability, *J. Climate*, 28, 3650-3670. <https://doi.org/10.1175/JCLI-D-14-00369.1>, 2015.
- Nihashi, S., Ohshima, K. I., and Tamura, T.: Sea-Ice Production in Antarctic Coastal Polynyas Estimated From AMSR2 Data and Its Validation Using AMSR-E and SSM/I-SSMIS Data. *IEEE JSTARS*, 10, 3912-3922. <https://doi.org/10.1109/JSTARS.2017.2731995>, 2017.
- Orsi, A. H., Johnson, G. C., and Bullister, J. L.: Circulation, mixing, and production of Antarctic Bottom Water. *Prog. Oceanogr.*, 43, 55-109. [https://doi.org/10.1016/S0079-6611\(99\)00004-X](https://doi.org/10.1016/S0079-6611(99)00004-X), 2019.
- Ohshima, K. I., Fukamachi, Y., Williams, G. D., Nihashi, S., Roquet, F., Kitade, Y., Tamura, T., Hirano, D., Herranz-Borreguero, L., Field, I., Hindell, M., Aoki, S. and Wakatsuchi, M. L.: Antarctic Bottom Water production by intense sea-ice formation in the Cape Darnley polynya. *Nat. Geosci.*, 6, 235-240. <https://doi.org/10.1038/ngeo1738>, 2013.
- Park, J., Kim, H.-C., Jo, Y.-H., Kidwell, A., and Hwang, J.: Multi-temporal variation of the ross sea polynya in response to climate forcings. *Polar Res.*, 37, 1444891. <https://doi.org/10.1080/17518369.2018.1444891>, 2018.
- Parkinson, C. L.: A 40-y record reveals gradual Antarctic sea ice increases followed by decreases at rates far exceeding the rates seen in the Arctic. *P. Natl. Acad. Sci. U.S.A.*, 116, 14414-14423. <https://doi.org/10.1073/pnas.1906556116>, 2019.
- Parmiggiani, F.: Fluctuations of Terra Nova Bay polynya as observed by active (ASAR) and passive (AMSR-E) microwave radiometers, *Int. J. Remote. Sens.*, 27:12, 2459-2467. <https://doi.org/10.1080/01431160600554355>, 2007.
- Preußner, A., Heinemann, G., Willmes, S., and Paul, S.: Multi-Decadal Variability of Polynya Characteristics and Ice Production in the North Water Polynya by Means of Passive Microwave and Thermal Infrared Satellite Imagery. *Remote Sensing*, 7, 15844-15867. <https://doi.org/10.3390/rs71215807>, 2015.
- [QGIS.org](http://www.qgis.org): QGIS Geographic Information System. QGIS Association. <http://www.qgis.org>, 2021.
- Rack, W., Price, D., Haas, C., Langhorne, P. J., and Leonard, G. H.: Sea Ice Thickness in the Western Ross Sea. *Geophys. Res. Lett.*, 48, e2020GL090866. <https://doi.org/10.1029/2020GL090866>, 2020.
- Rignot, E., Mouginot, J., Scheuchl, B., van den Broeke, M., van Wessem, M. J., and Morlighem, M.: Four decades of Antarctic ice sheet mass balance from 1979–2017. *P. Natl. Acad. Sci. U.S.A.* 116, 1095-1103. <https://doi.org/10.1073/pnas.1812883116>, 2019.
- Sansiviero, M., Morales Maqueda, M. Á., Fusco, G., Aulicino, G., Flocco, D., and Budillon, G.: Modelling sea ice formation in the Terra Nova Bay polynya. *J. Marine Syst.*, 166, 4-25. <https://doi.org/10.1016/j.jmarsys.2016.06.013>, 2017.
- Spreen, G., Kaleschke, G. L., and Heygster, G.: Sea ice remote sensing using AMSR-E 89 GHz channels. *J. Geophys. Res.*, 113, C02S03. <https://doi.org/10.1029/2005JC003384>, 2008.
- Stammerjohn, S. E., Maksym, T., Massom, R. A., Lowry, K. E., Arrigo, K. R., Yuan, X., Raphael, M., Randall-Goodwin, E. R., Sherrell, R. M., and Yager, P. L.: Seasonal sea ice changes in the Amundsen Sea, Antarctica, over



- 944 the period of 1979–2014. *Elementa: Science of the Anthropocene*, 3, 000055. <https://doi.org/10.12952/journal.elementa.000055>, 2015.
- 945
- 946
- 947 St-Laurent, P., Yager, P. L., Sherrell, R. M., Stammerjohn, S. E., and Dinniman, M. S.: Pathways and supply of dissolved iron in the Amundsen Sea (Antarctica), *J. Geophys. Res.-Oceans*, 122, 7135–7162, <https://doi.org/10.1002/2017JC013162>, 2017.
- 948
- 949
- 950
- 951 St-Laurent, P., Yager, P. L., Sherrell, R. M., Oliver, H., Dinniman, M. S., and Stammerjohn, S. E.: Modeling the seasonal cycle of iron and carbon fluxes in the Amundsen Sea Polynya, Antarctica. *J. Geophys. Res.: Oceans*, 124, 1544–1565. <https://doi.org/10.1029/2018JC014773>, 2019.
- 952
- 953
- 954
- 955 Sweeney, C.: The annual cycle of surface water CO₂ and O₂ in the Ross Sea: A model for gas exchange on the continental shelves of Antarctica, in *Biogeochemistry of the Ross Sea. Antarctica Research Series*, 78, edited by Dunbar, R. B., and DiTullio, G. R., pp. 295–312, AGU, Washington, D. C., 2003.
- 956
- 957
- 958
- 959 Tamura, T., Ohshima, K. I., and Nihashi, S.: Mapping of sea ice production for Antarctic coastal polynyas, *Geophys. Res. Lett.*, 35, L07606. <https://doi.org/10.1029/2007GL03290>, 2008.
- 960
- 961
- 962 Tamura, T., Williams, G. D., Fraser, A. D., and Ohshima, K. I.: Potential regime shift in decreased sea ice production after the Mertz Glacier calving. *Nat. Commun.*, 3, 826. <https://doi.org/10.1038/ncomms1820>, 2008.
- 963
- 964
- 965 Tian, L., Xie, H., Ackley, S. F., Tang, J., Mestas-Núñez, A. M., and Wang, X.: Sea-ice freeboard and thickness in the Ross Sea from airborne (IceBridge 2013) and satellite (ICESat 2003–2008) observations. *Ann. Glaciol.*, 61(82), 24–39. <https://doi.org/10.1017/aog.2019.49>, 2020.
- 966
- 967
- 968
- 969 Webber, B. G. M., Heywood, K. J., Stevens, D. P., Dutrieux, P., Povl Abrahamsen, E., Jenkins, A., Jacobs, S. S., Ha, H. K., Lee, S. H., and Kim, T. W.: Mechanisms driving variability in the ocean forcing of Pine Island Glacier, *Nat. Commun.*, 8, 14507. <https://doi.org/10.1038/ncomms14507>, 2017.
- 970
- 971